Constraining the origin and influence of andesite in the Purico ignimbrite, Northern Chile

Sarah Lapinski

A senior thesis completed in the College of Earth, Ocean, and Atmospheric Science at Oregon State University

June 5th 2020

Advisors:

Shanaka de Silva, CEOAS, OSU

Dale H. Burns, Earth and Planetary Sciences, Stanford University

Table of Contents

List of Figures

List of Tables

Abstract

A feature of large continental magmatic systems is voluminous dacite ignimbrites erupted from upper crustal magma reservoirs. In the Altiplano Puna Volcanic Complex (APVC) of the Central Andes, a major ignimbrite and caldera plateau, magma systems are found to be long-lived and remarkably homogeneous requiring that they be maintained by recharge at depth. The characteristics of the recharge magma is poorly constrained because it is rarely erupted due to density and viscosity barriers in the magmatic system. An exception is the 1 Ma Purico ignimbrite (~100 km^3), where andesite appears late in the dominantly crystal-rich dacite climactic eruption and becomes dominant in post-climactic effusive eruptions.

The andesitic pumice (60 to 62% SiO_2) and bands in mixed pumice are microvesicular and contain a phenocryst assemblage of plagioclase, orthopyroxene, clinopyroxene, magnetite and ilmenite ± amphibole, biotite and quartz. Glomerocrysts of opx, cpx, and plagioclase are common. Two compositionally and isotopically distinct types of plagioclase, small (<500 μm) subhedral to euhedral crystals with high MgO (130-490 ppm) and low $^{87}Sr/^{86}Sr$ crystals (0.7076-0.7084) record a hot (>900 °C) andesite magma derived from an ~20 km deep magma reservoir. In contrast, the second type of plagioclase in the andesite appear to broken fragments of larger crystals and have significantly lower MgO (90-240 ppm), higher $^{87}Sr/^{86}Sr$ (0.7096-0.7114), and record cooler ~800-900 °C, upper crustal <10 km conditions.

The presence of touching orthopyroxene and clinopyroxene pairs coupled with iron-titanium oxide pairs throughout the andesite samples were observed and used to conduct thermobarometric modeling to uncover a warmer ~900-1100°C magma reservoir with middle crustal 15-35 km conditions.

The compositional variations observed in plagioclase crystals from the Purico andesitic pumices and the touching pyroxene pairs record recharge of a previously emplaced upper crustal (4-8 km depth) dacite magma reservoir by andesite coming from deep (~20 km). During ascent, the andesite incorporated crystals from the surrounding upper crustal plutonic bodies. Thus, the andesite itself is significantly modified and is a hybrid between a more mafic parent and upper crustal silicic melts.

Introduction

1.1 Geologic Setting

The Cerro Purico Volcanic Complex (CPVC) is situated in the larger Central Volcanic Zone (CVZ) in the Central Andes and is considered the last major eruptive center associated with the Altiplano-Puna Volcanic Complex (APVC; de Silva 1989; Figure 1). The APVC has been subjected to magmatism migrating westward that is a result of ~200 million years of eastward subduction of the Nazca plate producing one of the most productive volcanic provinces in the world (Rogers and Hawkesworth 1989). In the Neogene, some of the largest eruptions in Earth's history occurred throughout the Central Andes forming the Central Andean Neogene Ignimbrite Province (de Silva et. al. 2006). The APVC is one of the most intense areas of volcanism which was formed ~25 Ma due to crustal shortening that continued until at least ~ 10 Ma resulting in crust thicknesses > 70 km beneath the APVC (Burns et al., 2015).

Continental volcanic arcs exhibit cyclic and episodic behavior that are dominated by steady, low volume magmatism (steady-state volcanism) with short lived high-intensity flare-ups; magma production rates were 3-4 times higher than those at steady state in the APVC (Ducea 2001, de Silva et. al., 2007, DeCelles et. al., 2009, Folks et. al., 2011a, Burns et. al. 2015). Crustal shortening in the APVC occurred simultaneously with a magmatic flare up between 10-1Ma that erupted in four main pulses 10, 8, 6, and 4 Ma which generated significant volumes of silicic magma (Lipman 2007, de Silva 2008, Salisbury et. al., 2011, Best et. al., 2013, Burns et. al. 2015). The flare-up event in the APVC is a result of a high influx of mantle-derived magma due to the steepening of the subduction angle of the Nazca plate, influencing the main construction of the cordilleran batholiths and the caldera field that comprises the APVC (Best et. al. 1**991**, Ducea 2001, de Silva et. al., 2006a, de Silva et. al. 2007). The APVC is dominated by tens-of-thousands of cubic kilometers of ignimbrites during flare-up events and form multiple caldera complexes that are spatially and temporally related. These intense periods of volcanism result in ignimbrite eruptions and calderas that dominate the landscape (Figure 2).

The ignimbrites found in the APVC are orders of magnitude larger than typical arc eruptions both in the CVZ and throughout the world. The presence of this abnormally high intensity volcanic field within the CVZ makes the region an important study area to better understand large caldera eruptions.

Calderas are found to be underlain by a large seismic low velocity zone interpreted to represent the remnants of the magma complex formed from the steepening of the subduction angle that fed the caldera-forming super eruptions of the APVC (Figure 3a; Ward et. al. 2004, Zandt et. al. 2003). This low velocity zone beneath the APVC is thought to be a 5000km^3 MASH (Melting, Assimilation, Storage, and Homogenization) zone referred to as the Altiplano Puna Magma Body (APMB) seen as the red shape in Figure 3b, defined within the 2.9 km/sec contour and likely has ~20% melt (Ward et. al. 2004). Upper crustal MASH zones such as the APMB are thought to supply recharge magma for large caldera zones, however the geochemical makeup and true influence are poorly constrained.

1.2 Cerro Purico Volcanic Complex

The CPVC is an example of the many long lived silicic volcanic complex's in the APVC (Figure 4). This caldera erupted large volumes of silicic ignimbrites from ~1Ma to 0.2Ma during the transition from the 10-1 Ma ignimbrite flare-up in the APVC to steady state arc volcanism and represents the last major ignimbrite eruption in the region (de Silva, 1991, Schmitt et. al. 2001, de Silva 2007). The dominantly dacitic ignimbrite from the most recent Purico ~1Ma eruption contained andesitic pumice and 20% basaltic andesite inclusions in the waning stages of its most recent activity (Schmitt et. al. 2001, Burns et al., 2015).

The Purico ignimbrite is composed of 3 distinct flows and reflects the compositionally zoned silicic magma reservoir beneath the CPVC (Spera et. al., 1981, de Silva 1991, Eichelberger et. al., 2000, Coleman et. al. 2012). The Lower Purico Ignimbrite I is composed of a homogenous dacite, Lower Purico Ignimbrite 2 contains a surge deposit and rhyolite fall pumice overlain by dacite and a dacite-andesite

banded pumice (Figure 5). The rhyolite, dacite, and andesite in the Purico ignimbrite have indistinguishable Nd and Sr isotopic compositions, however geothermometry on the three pumice types show that the dacite formed in relatively constant temperatures (780°C-800°C) while the rhyolite and andesites yield significantly higher temperatures (850°C -950°C) (Schmitt et. al. 2001). Furthermore, crystal isotopic variations in the andesite show that there are two distinct plagioclase types, a depleted $^{87}Sr/^{86}Sr$ (0.7076-0.7084) with MgO (130-490 ppm) plagioclase and high $^{87}Sr/^{86}Sr$ (0.7096-0.7114) low MgO (90-240 ppm) plagioclase (Burns et. al., 2015). The isotopically depleted crystals likely reflect the mid-crustal magma that supplied magma to the upper crust prior to the Purico ignimbrite eruption (Godoy et. al. 2019). The compositional differences between the dacite and andesite, and the crystal composition variations in the andesite served as the motivation for this study to constrain the origin and influence of the andesite in the CPVC.

2. Approach and Methods

2.1 Fieldwork and Sample Collection

Andesite samples collected by Shanaka de Silva and Dale Burns in the CPVC in northern Chile were used for the analysis in this project. Supplemental field work was conducted in August 2019 to collect more andesite pumice samples at -23°S -67.75°W in Chile. The location of each sample collected in 2019 was found using a remote GPS unit.

2.2 Whole rock major and trace element analysis: X-Ray Fluorescence (XRF) and ICP-MS

Seven andesite samples and two banded andesite-dacite samples with little weathering were selected for analysis. Each sample was crushed using steel plates in the jaw-crusher and milled into a fine powder at Oregon State University and brought to the Peter Hooper GeoAnalytical Lab at Washington State University for analysis preparation. XRF analysis on each sample were conducted using a ThermoARL AdvantXP machine requiring each sample to be combined with a lithium flux in a 2:1 ratio and fused into a bead. The bead is then polished prior to analysis. The samples prepared for XRF

analysis were also analyzed in the Peter Hooper GeoAnalystical Lab using a Finnigan Element2 ICP-MS for REE and trace elements. All methods follow thise described by Johnson et al. (1999).

2.3 Electron Probe Micro-Analysis (EPMA)

Four representative pumice samples were selected and cut for thin section preparation at Spectrum Petrographics in Vancouver, Washington. These thin sections were then analyzed using the CAMECA SX-100 electron microprobe (EMP) at Oregon State University. The EMP is equipped with five wave-length-dispersive spectrometers (WDS) and high-intensity dispersive crystals for high-sensitivity trace element analysis. Minerals and groundmass glasses were analyzed using 15 keV accelerating voltage, 30nA sample current, and 1 um beam diameter for mineral phase and 5 μm for groundmass glasses (Electron Microprobe Laboratory, 2016). Supplemental EPMA data was provided by Dale Burns.

3. Results

3.1 Lithology and whole rock textures

The three distinct types of pumice were found in the Lower Purico II flow unit and were the focus of this study. All of the Purico pumices were composed of porphyritic, microvesicular, non-welded pumice with vesicles ranging from 20um to 400um in diameter (Figure 6).

The basal fall unit was composed of crystal-poor (<10%) rhyolite pumice consisting of phenocrysts of plagioclase, biotite, quartz, and oxides (Burns et. al., 2015). The overlaying dacite pumice contains phenocrysts of plagioclase, amphibole, biotite, quartz, minor orthopyroxene, and clinopyroxene. The pumice in the upper third section of this flow unit is crystal rich (~50-60% crystals) dark glassy pumice containing phenocrysts and glomerocrysts of plagioclase, clinopyroxene, orthopyroxene, and Fe-Ti oxides. The mingled andesite-dacite portion of the flow unit contained dark and light glassy pumices which were distinguished through geochemical analysis.

The dark glassy pumice's contained ~15% glomerocrysts of the described mineralogy while the light glassy pumice contained ~25% glomerocrysts (Figure 7). The banded samples contained a similar mineral assemblage with a lack of glomerocrysts seen in the other end members and contained minor (~5%) amphibole that was not observed in the light and dark end members. These bands range from 2mm-2cm bands of mingled dark and light glassy pumice (Figure 6).

3.2 Whole Rock Chemistry

The samples analyzed in this study are composed of both dacite and andesite. The dacite samples in this study were found as bands in the banded andesite (Figure 6d) and cover a restricted compositional gap (63%-64% SiO_2) while the andesite covered a large compositional gap between 59% - 62.0% SiO_2 (Figure 8).

The Purico andesites are among the most mafic samples in the APVC. While the CPVC has erupted a large range of compositions throughout it's activity, the most mafic andesite in this study is composed of some of the most mafic material in the APVC (Table 1).

3.3 Summary of Dacite and Andesite Petrology

The andesite and dacite contain similar mineral assemblages (Table 2). The andesitic pumice contains ~5% more glomerocrysts and phenocrysts and are lacking in amphibole. The dacite samples contain ~45% crystals, ~40% glass, and ~15% vesicles. The dominant phenocryst and glomerocryst phases in the dacite include ~75% plagioclase, ~20% pyroxene, and ~5% Fe-Ti oxides with minor amphibole. Glass and oxide inclusions were observed in all of the plagioclase and pyroxenes. The andesite contained ~40% crystals, 45% glass, and 15% vesicles. The dominant crystal phases include ~60% plagioclase, ~30% pyroxenes, and 5% Fe-Ti oxides found as phenocrysts and in glomerocrysts (Figure 7). Glass and oxide inclusions were found in the plagioclase and pyroxenes in similar quantities as the dacite. There were two types of banded andesite found within the andesitic pumice lens. Banded Andesite Type 1 (BA1) contained ~60% crystals, 30% glass, and 10% vesicles with a similar

mineralogy to the andesite with the inclusion of ~16% amphibole. In contrast, the banded andesite type 2 (BA2) had significantly more glass and vesicles and only contained plagioclase (80%) and biotite (20%). There was a notable absence of glomerocrysts in both BA1 and BA2.

3.4 Phenocryst Textures and Compositional Patterns

3.4.1 Plagioclase

Plagioclase from the Purico andesite pumice are found as individual phenocrysts and in glomerocrysts with CPX and OPX. Three textural types of plagioclase were observed, however no significant compositional differences were found between the textural types (Figure 9). Furthermore, all textural types were observed in both phenocrysts and glomerocrysts. While there were no distinguishable compositional or textural differences in the crystals found as phenocrysts and glomerocrysts, two compositional types were observed throughout the andesite.

Plagioclase in the glomerocrysts range in size from ~200-500 microns, are subhedral, and show minor sieve textures in both crystal interiors and crystal rims (Figure 9a). Compositionally, crystal interiors define a wide range of An contents (An56-82). Close inspection of these interiors reveal two distinct compositional types of plagioclase within the phenocrysts and glomerocrysts.

Plagioclase type 1 (P1) have significantly higher An contents (An69-82 vs An55-68) with higher MgO and FeO concentrations then plagioclase type 2 (P2). Both P1 and P2 plagioclase have compositionally indistinguishable, ~20um thick rims that range from An(68-82) with a range of MgO and FeO (Table 2, Figure 10).

Plagioclase phenocrysts range in size from 200-500 um, are subhedral, and show a range of sieve textures in both the crystal interiors and the rims. The large >500um phenocrysts show major sieve textures. Compositionally, the crystal interiors show a wide range of An content (An43-82). The two compositional types of plagioclase were observed as phenocrysts.

While the glomerocrysts analyzed have slightly higher An content and MgO, there is no distinct compositional or textural differences between the crystals found as phenocrysts and glomerocrysts in the andesite (Table 3).

3.4.2 Pyroxene

Pyroxene was observed in 2 dominant phases in both the andesite and dacite. Clinopyroxene (CPX) was found as augite determined through EMP analysis with a modal abundance of 10% in both the dacite sample and the andesite. Orthopyroxene (OPX) was found as hypersthene determined through EMP analysis with a modal abundance of about 15% in andesite and about 10% in dacite (Figure 11). These minerals were often found as touching pairs in all andesite samples (Figure 12).

Clinopyroxene

Clinopyroxene from the Purico andesite pumice are found as both individual phenocrysts and in glomerocrysts with plagioclase and OPX. CPX were found as Augite with a range in En and Fs (Figure 11). Textural differences between the phenocrysts and glomerocrysts are distinct however there is no compositional variability in the pumice.

CPX phenocrysts were observed in two distinct textural types (Figure 13). Type I phenocrysts range in size from ~200-300um, contain many melt and oxide inclusions, and display significant sieve textures in the crystal rims. Type 2 phenocrysts range ~50-200um and contain few melt inclusions with minor sieve texture. There are compositionally indistinguishable with Wo content of (39.6-20.2) and Mg# 75-76.

CPX in the glomerocrysts had a small range of pyroxene textures and compositional variation with Wo contents of 39-40.5 and a Mg# ranging from 72-76. Minor sieve textures and Fe-Ti oxide inclusions were observed in all CPX in the glomerocrysts.

There were no distinct compositional difference between the clinopyroxene found as phenocrysts or glomerocrysts (Figure 14). However, the glomerocrysts had a slightly larger range of Mg#

which contained both the highest and lowest Mg# indicating a larger range of magnesium content in the magma that the glomerocrysts formed in.

Orthopyroxene

The orthopyroxene in this sample were also found as phenocrysts and in glomerocrysts with plagioclase and CPX. Both types of OPX were found as hypersthene. While the OPX crystals varied in size there were no significant textural differences observed (Figure 15).

The OPX found in dacite had Wo content of 2.20-2.35 with an Mg# between 69.2-72.3. The andesitic samples yielded Wo contents of 1.76-3.77 with an Mg# between 68.3-74. The glomerocrysts and phenocrysts had slight differences in composition (Figure 16). The glomerocrysts had a larger range of Mg# in both the cores and the rims. The rims had a compositional range of Mg# between 67-77 while the phenocryst rims had a compositional variation of Mg# between 72-75.

3.4.3 Iron-Titanium Oxide

The Iron-titanium oxides in the andesite samples were found as ~60% phenocrysts, ~20% glomerocrysts, ~15% inclusions in plagioclase and pyroxene, and ~5% as homogeneous oxide glomerocrysts. EMP analyses showed that majority of the phenocrysts were magnetite with TiO_2 wt% ranging from 6-18%. Ilmenite was isolated in glomerocrysts and inclusions in pyroxene with TiO_2 wt% ranging from 38 to 43% (Figure 17).

4. Modeled Intensive Parameters

4.1 Pressure and Temperature (P-T)

4.1.1 Pyroxene

The pressure and temperature conditions of the Purico andesite is vital to understanding the relationship and source of the andesite and dacite in this system. Keith Putirka's 2003 2 pyroxene thermobarometer and the cpx-melt thermobarometer were utilized to yield model estimates of

pressure and temperature crystallization of the pyroxene (Putirka 2008). Equation 36 was used for 40% of the pairs where the Mg# of CPX was greater than 0.75, equation 37 was used for the remaining 60% of pairs with lower Mg#. Equation 39 was then used to calculate the pressure for the pairs with a K_D value <1.09. The K_D values of all pairs were less than 1.02. Most pyroxenes are in equilibrium due to the Fe-Mg exchange with any glass composition (Roeder and Emslie, 1970). In order to investigate the differences between the andesite and dacite, published data used Putirka's plagioclase-amphibole pairs to yield model estimates of the pressure and temperature conditions of minerals in the dacite. The model indicates that minerals in the andesite were formed at significantly higher pressure and temperature conditions compared to the dacite. Sufficient data was not collected on the andesite pyroxene phenocrysts in order to compare the different crystallization conditions between phenocrysts and glomerocrysts within the andesite, however the P-T conditions of the glomerocrysts were calculated. The 2-pyroxene thermobarometry contain errors between 10-40 °C and 1-2 kilobars. The clinopyroxene-liquid thermobarometry yielded results with errors between 30-50 °C and 2-4 kilobars.

4.1.2 Oxides

ILMAT iron-titanium oxide thermometer was used to look at the relationship between temperature and oxygen fugacity of oxides from pyroxene inclusions, glomerocrysts, and homogenous oxide clots in the andesite. Oxygen fugacity refers to the chemical potential of oxygen in the magma which can be used to model the temperature in which the oxides formed. ILMAT uses the average temperature and logarithmic oxygen fugacity calculated by Carmichael 1967, Anderson 1968, Lindsley & Spencer 1982 and Stormer 1983 to model the conditions of crystallization of the Fe-Ti pairs. For the purpose of this study the calculated temperatures are used to investigate the magma conditions of the andesite. This model yielded significant differences in temperature between the different groups with an error of 50°C and log fO_2.

5. Discussion

5.1 Plagioclase

The anorthite (An) and MgO content of the two plagioclase types in the Purico andesite suggest that the plagioclase crystalized in two different temperature conditions. P1 formed in a high temperature environment indicated by the high An content while P2 formed in lower temperature conditions (Figure 18a). The glomerocrysts did not display significant differences in An content signifying that they formed in similar conditions to the phenocrysts (Figure 18b).

The P2 andesite plagioclase that plot between 2% and 3% MgO likely represents magma mixing that occurred between the andesite and dacite prior to eruption. The remaining P2 that crystalized in a spread of magma compositions likely represent crystals that formed through fractional crystallization of the andesite. The P1 plot significantly higher MgO% between 3% and 8%. This displays a range of crystallization conditions with the most mafic plagioclase crystallizing in basaltic andesitic magma. These highly mafic plagioclases may represent crystals from a more primitive magma that feeds the system.

5.2 Pyroxene

There was not a significant amount of variation in composition between the phenocrysts and glomerocrysts of both pyroxene minerals. The mineral assemblage of the andesite shows that there is significantly more pyroxene present in glomerocrysts (~80%) than in the phenocryst phase (~20%). The glomerocrysts contain slightly lower Mg# compared to the phenocrysts. These factors indicate that there were more pyroxenes crystalizing when the glomerocrysts were formed. The thermobarometry calculations show that the andesite pyroxene glomerocrysts crystallized at between 950-1050°C and pressures ~4.50-11 kilobars which is significantly higher than the amphibole-plagioclase of the dacite which crystalized between 1-2 kilobars and 800-900°C. The pyroxene pairs in the glomerocrysts crystallized in a large range of pressures likely tracking the ascent of the magma through the upper crust (Figure 19).

5.3 Fe-Ti Oxides

Thermometry calculations conducted on touching Fe-Ti pairs showed three separate crystallization temperatures for the 3 touching pair types (Figure 20). Oxides paired with glomerocrysts yielded crystallization temperatures of 850-950°C concordant the crystallization temperatures calculated with the two pyroxene pairs from the same glomerocryst. Oxide pairs found as inclusions crystalized at a larger range of temperatures between 880-1050°C, while andesitic homogenous oxide clot crystalized at 930°C. The homogenous clot found in the dacitic band crystallized at a significantly lower temperature of 790°C likely reflecting the temperature of the dacite magma chamber prior to magma mingling. The varying temperatures represent the various crystallization conditions of the oxide pairs. Oxide inclusions in high temperature pyroxenes were crystallized at greater depths near the source of the andesite, while the oxides in glomerocrysts and in homogeneous oxide clots represent fractional crystallization of the andesite as it moved through the system.

5.4 Magma Dynamics

While the dacite represents the pre-eruption uppermost crustal reservoir, the andesite in the CPVC clearly represents material from a upper-crustal reservoir. The trace element composition of plagioclase, thermobarometric modeling of pyroxenes and dacitic plagioclase, and oxygen fugacity modeling of Fe-Ti oxides support Burns et. al. (2012) model of a deeper andesitic source between 15-35km depth in a higher temperature magma reservoir. The lower An content in the dacite indicate that the dacite crystalized in a much lower pressure and temperature crystallization environment consistent with an upper crustal magma reservoir. Plagioclase-amphibole thermobarometry indicates that the dacitic magma crystallized between 0-2 km depth. Burns et. al. (2015) found the $^{87}Sr/^{86}Sr$ ratio of the plagioclase in the dacite to be 0.7087-0.7090 congruent with upper crustal evolution while the andesite had lower $^{87}Sr/^{86}Sr$ isotope ratios (0.7076-0.7084). This combined with the 2-pyroxene thermobarometry indicates the pyroxenes in the andesite originate between 15-35 km depth that is consistent with the geophysical estimated depth of the Altiplano Magma Body (APMB), a crystal mush of plagioclase,

pyroxene, and oxides that fractionated to produce more silicic melts (Figure 21). While there were not significant compositional differences between the phenocrysts and glomerocrysts of each mineral, the composition of the 2 plagioclase types and pyroxene thermobarometry show that the glomerocrysts and some of the phenocrysts recorded crystallization of pyroxenes in the crystal mush and their ascent to the surface.

6. Conclusions and Future Work

The andesite found in the ~1Ma Purico ignimbrite is small sample of the large APMB that lies beneath the entire APVC. This late andesitic eruption provides a rare look into the APMB and gives geochemical insight into the likely source of recharge for the large caldera-forming eruptions. The plagioclase compositions and the thermobarometric modeling in this study support Burns et. al. (2015) model of a previously emplaced dacitic magma reservoir that the hotter (~100°C) andesite intercepted prior to the Purico ignimbrite eruption. By understanding the geochemical makeup of the APMB a more comprehensive model of the large-scale magma dynamics of the APVC can be built. The Purico ignimbrite contains some of the first geochemical evidence of the APMB and makes Purico an important case study to better understand the interworking's of this region of the Central Andes.

More detailed EMPA analyses coupled with laser ablation using the IC-PMS at Oregon State University of the phenocrysts and glomerocrysts in the Purico andesite will be conducted to investigate the differences between the two compositional plagioclase types and the differences between phenocrysts and glomerocrysts. These analyses will then be compared to the other andesites found in the APVC to investigate the relationship between the material from the APMB and the rest of the mafic material found in the APVC.

Acknowledgements

I would like to thank my advisors Shanaka de Silva and Dale Burns for their vast insight and dedication for the Cerro Purico Volcanic Complex and the support they've provided throughout the past 2 years. I would like to thank the VIPER group at OSU for their invaluable knowledge and input towards my understanding of volcanology, especially Katharine Solada who provided an immense amount of support as I transitioned to Oregon State as a researcher. Lastly, I would like to thank Chuck Lewis who helped me with field work, data analysis, and has provided an immense amount of support as my friend and office mate.

References

Anderson, A.T., 1968. Oxidation of the La Blanche Lake titaniferous magnetite deposit, Québec. Journal of Geology 76 (4), 528-547.

Andersen, D.J., Lindsley, D.H., 1985. New (and final!) models for the Ti-magnetite/ilmenite geothermometer and oxygen barometer. Abstract AGU 1985 Spring Meeting Eos Transactions. American Geophysical Union, v. 66 (18), p. 416, doi: .

Best, M. G., and Christiansen, E. H. 1991, Limited extension during peak Tertiary volcanism, Great Basin of Nevada and Utah, *J. Geophys. Res.*, v. 96(B8), p. 13509– 13528, doi:10.1029/91JB00244

Burns, D.H., de Silva, S.L., Tepley, F., Schmitt, A.K., and Loewen, M.W., 2015, Recording the transition from flare-up to steady-state arc magmatism at the Purico-Chascon volcanic complex, northern Chile: Earth and Planetary Science Letters, v. 422, p. 75–86, doi:10.1016/j.epsl.2015.04.002.

Carmichael, I.S.E., 1967. The iron-titanium oxides of salic volcanic rocks and their associated ferromagnesian silicates. Contributions to Mineralogy and Petrology, v. 14 (1), p. 36-64, doi: 10.1007BF00370985.

Coleman, D.S., Bartley, J.M., Glazner, A.F., and Pardue, M.J., 2012, Is chemical zonation in plutonic rocks driven by changes in source magma composition or shallow-crustal differentiation? Geosphere, v. 8, p. 1568–1587, doi:10.1130/GES00798.1.

DeCelles, P. G., Ducea, M. N., Kapp, P. & Zandt, G., 2009, Cyclicity in Cordilleran orogenic systems. *Nature Geoscience, v.* **2**, p. 251–257, doi: 10.1038ngeo469

de Silva, S.L., 1991, Style of zoning in central Andean ignimbrites; Insights into magma chamber processes: Geological Society Special Publication, p. 217–232

de Silva, S.L., Zandt, G., Trumbull, R., Viramonte, J.G., Salas, G., Jiménez, 2006, Large ignimbrite eruptions and volcano-tectonic depressions in the Central Andes: a thermomechanical perspective, Geological Society, v. 269, p. 47-63, doi: 10.1144/GSL.SP.2006.269.01.04

de Silva, S.L., and Gosnold, W.D., 2007, Episodic construction of batholiths: Insights from the spatiotemporal development of an ignimbrite flare-up: Journal of Volcanology and Geothermal Research, v. 167, p. 320–335, doi:10.1016/j.jvolgeores.2007.07.015de Silva, S., 2008, Arc magmatism, calderas, and supervolcanoes: Geology, v. 36, p. 671-672, doi:10.1007s0C445.

de Silva, S.L., and Kay, S.M., 2018, Turning up the heat: High-flux magmatism in the central andes: Elements, v. 14, p. 245–250, doi:10.2138/gselements.14.4.245.

Ducea, M.N., 2001, The California arc: thick granitic batholiths, eclogitic residues, lithospheric-scale thrusting, and magmatic flare-ups, GSA Today, v. 11 (11) p. 4-10, doi: 10.1130/1052-5173(2001)011%3c;0004:TCATGB%3e;2.0.CO;2

Eichelberger, J.C., Chertkoff, D.G., Dreher, S.T., and Nye, C.J., 2000, Magmas in collision: Rethinking chemical zonation in silicic magmas: Geology, v. 28, p. 603–606, doi:10.1130/0091 7613(2000)028<0603:MICRCZ>2.3.CO;2.

"Electron Microprobe Laboratory." *Oregon State University Advantage",* 19 Feb. 2016*,* advantage.oregonstate.edu/facilities/electron-microprobe-laboratory.

Folkes, C.B., De Silva, S.L., Schmitt, A.K., and Cas, R.A.F., 2011a, A reconnaissance of U-Pb zircon ages in the Cerro Galán system, NW Argentina: Prolonged magma residence, crystal recycling, and crustal assimilation: Journal of Volcanology and Geothermal Research, v. 206, p. 136–147, doi:10.1016/j.jvolgeores.2011.06.001.

Godoy, B., Taussi, M., González-Maurel, O., Renzulli, A., Hernández-Prat, L., le Roux, P., Morata, D., and Menzies, A., 2019, Linking the mafic volcanism with the magmatic stages during the last 1 Ma in the main volcanic arc of the Altiplano-Puna Volcanic Complex (Central Andes): Journal of South American Earth Sciences, v. 95, p. 102295, doi:10.1016/j.jsames.2019.102295.

Kern, J.M., de Silva, S.L., Schmitt, A.K., Kaiser, J.F., Iriarte, A.R. Economos, R., 2016, Geochronological imaging of an episodically constructed subvolcanic batholith: U-Pb in zircon chronochemistry of the Altiplano- Puna Volcanic Complex of the Central Andes, Geosphere, v. 12 (4), p. 1-24, doi: 10.1130/GES01258.1

Lepage, Luc D., ILMAT: an Excel worksheet for ilmenite magnetite geothermometry and geobarometry Department of Geological Sciences, Queens University, Kingston, Ont., Canada K7L 3N6, Computers and Geosciences, V 29,D 2003,8 June 01, 2003,P 673,%U https://ui.adsabs.harvard.edu/abs/2003CG ....29..673L, 10.1016/S0098-3004(03)00042-6

Lindsley, D.H., Spencer, K.J., 1982. Fe-Ti oxide geothermometry: Reducing analyses of coexisting Ti- magnetite (Mt) and ilmenite (Ilm) abstract AGU 1982 Spring Meeting Eos Transactions. American Geophysical Union 63 (18), 471.

Lipman, P.W., 2007, Incremental assembly and prolonged consolidation of Cordilleran magma chambers: Evidence from the Southern Rocky Mountain volcanic field. Geosphere, v. 3, p. 42-70 , doi: 10.1130/GES00061.1

Powell, R., Powell, M., 1977. Geothermometry and oxygen barometry using coexisting iron-titanium oxides: a reappraisal. Mineralogical Magazine 41 (318), 257-263.

Putirka, K.D., 2008, Thermometers and barometers for volcanic systems: Reviews in Mineralogy and Geochemistry, v. 69, p. 61–120, doi:10.2138/rmg.2008.69.3.

Salisbury, M.J., Jicha, B.R., de Silva, S.L., Singer, B.S., Jimẽnez, N.C., & Ort, M.H., 2011, 40Ar/39Ar chronostratigraphy of Altiplano-Puna volcanic complex ignimbrites reveals the development of a major magmatic province. Geological Society of America Bulletin, v. 123, p. 821-840., doi: 10.1130/B30280.1

Schmitt, A.K., de Silva, S.L., Trumbull, R.B., and Emmermann, R., 2001, Magma evolution in the Purico ignimbrite complex, northern Chile: Evidence for zoning of a dacitic magma by injection of rhyolitic melts following mafic recharge: Contributions to Mineralogy and Petrology, v. 140, p. 680–700, doi:10.1007/s004100000214.

Spencer, K.J., Lindsley, D.H., 1981. A solution model for coexisting iron-titanium oxides. American Mineralogist 66 (11-12), 1189-1201.

Spera, F.J., and Crisp, J.A., 1981, Eruption volume, periodicity, and caldera area: Relationships and inferences on development of compositional zonation in silicic magma chambers: Journal of Volcanology and Geothermal Research, v. 11, p. 169–187.

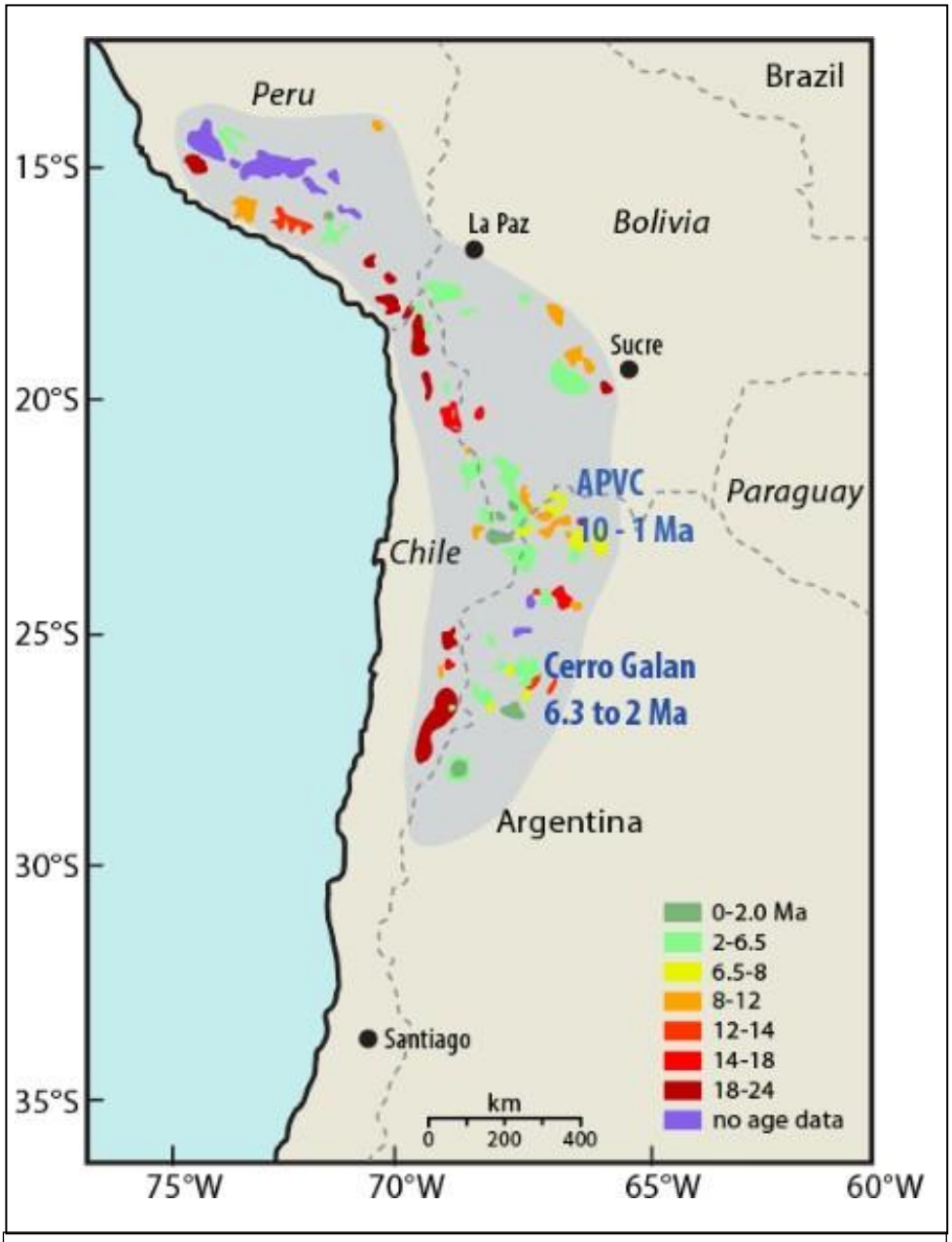

Figure 1. Map of the APVC in the Central Andes, S. America. The blue shaded area shows the boundary of the APVC. The colored fields represent the ages of the caldera's and their deposits (de Silva and Kay 2019).

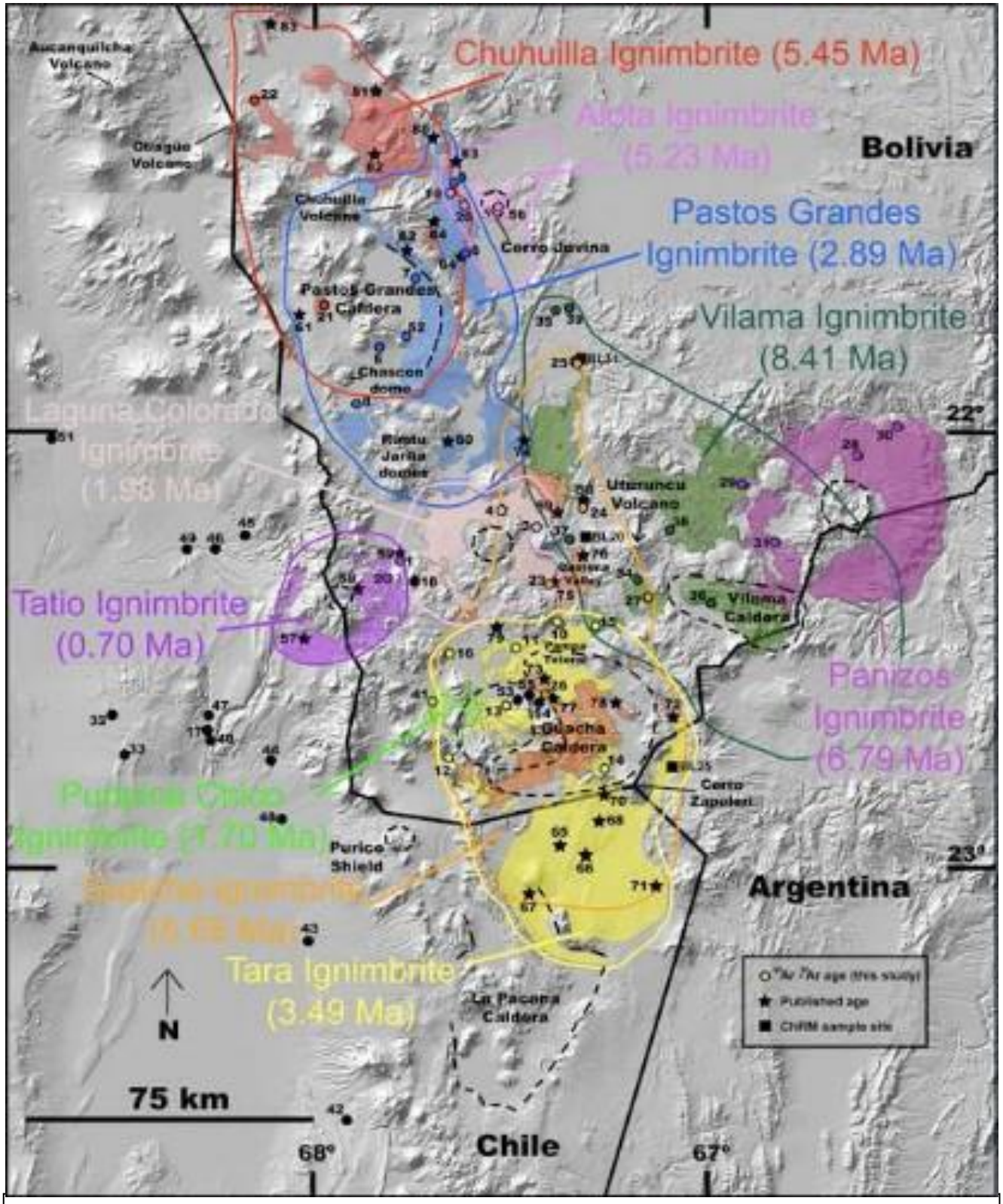

Figure 2. APVC ignimbrites and source calderas (Salisbury et. al. 2010). 2b. Shaded relief map of APVC. The warmer colors represent increasing elevation up to 6000m (Ward et. al. 2014).

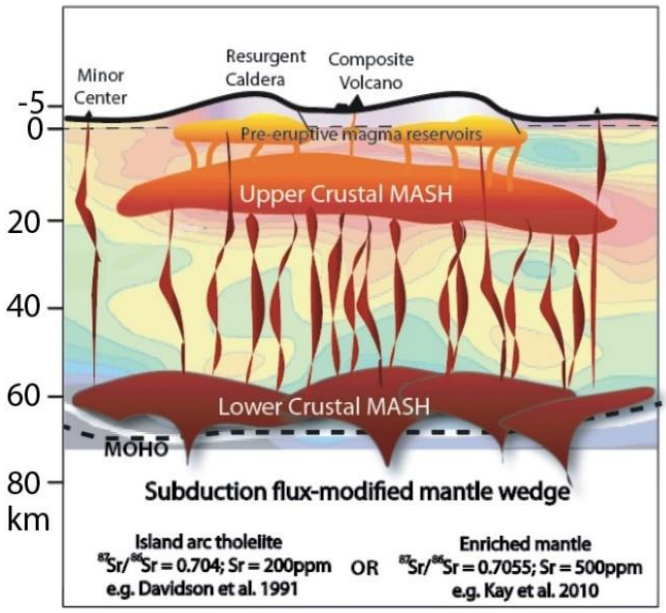

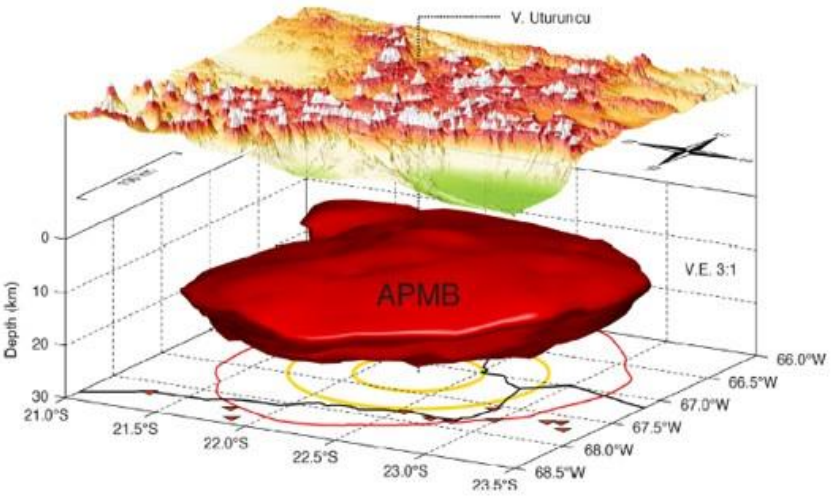

Figure 3. (a) Schematic cross section of the APVC displaying the upper crustal Altiplano Puna Magma Body (APMB) MASH (de Silva and Kay, 2019). (b) Geophysical model of the APMB beneath the APVC (Ward et. al. 2014).

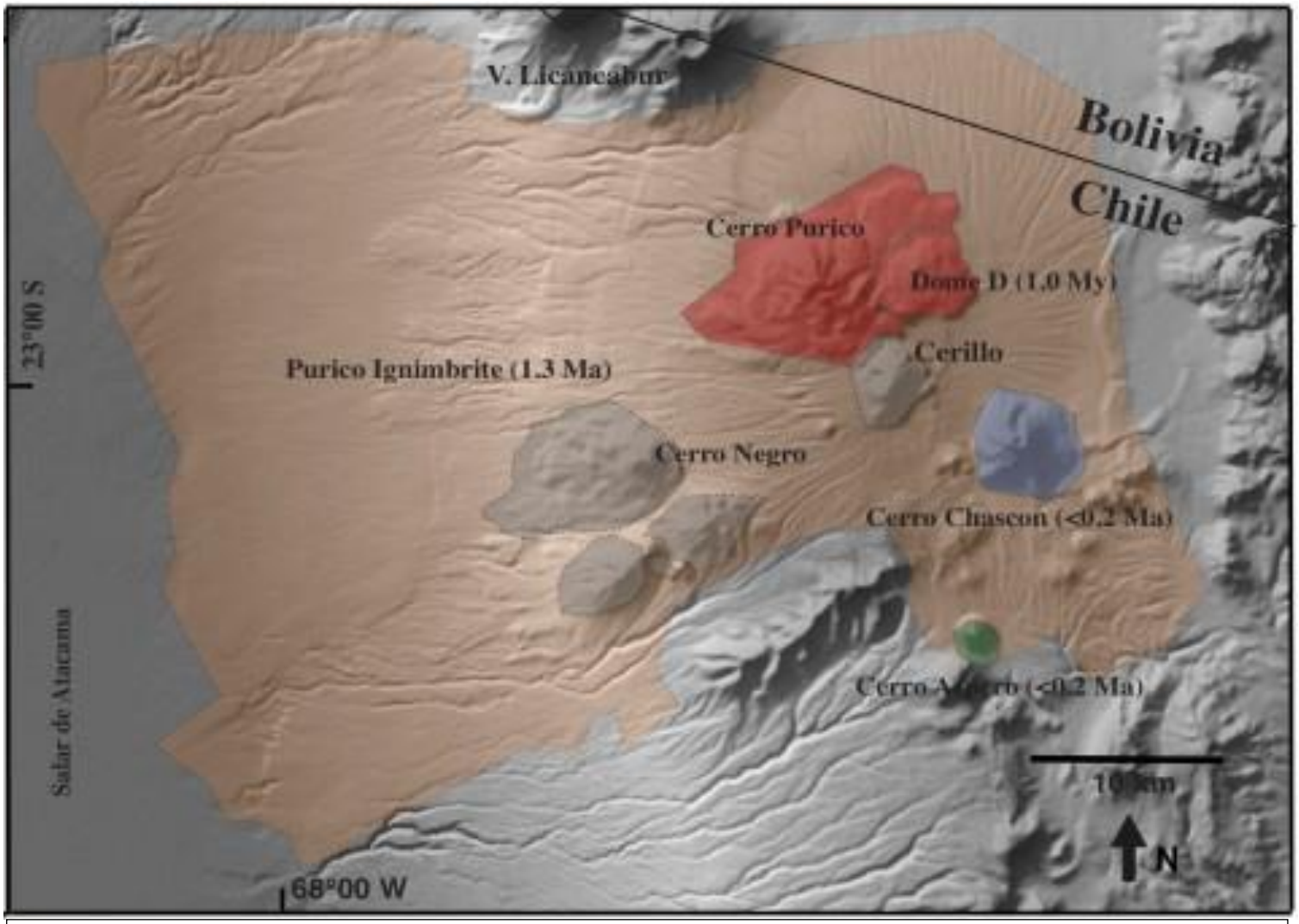

Figure 4. Areal map of the Purico Ignimbrite in tan with the surrounding caldera's in red, grey, blue, and green. The Cerro Purico Volcanic Complex (CPVC) is shaded red in the north eastern section of the map.

Figure 5. A schematic stratigraphic column (left) of the ~1Ma Purico ignimbrite with the field photograph (right) of the section. The andesite, dacite, and banded pumice in the study were collected from the upper third section of the Lower Purico Ignimbrite II flow unit (Burns et. al. 2015).

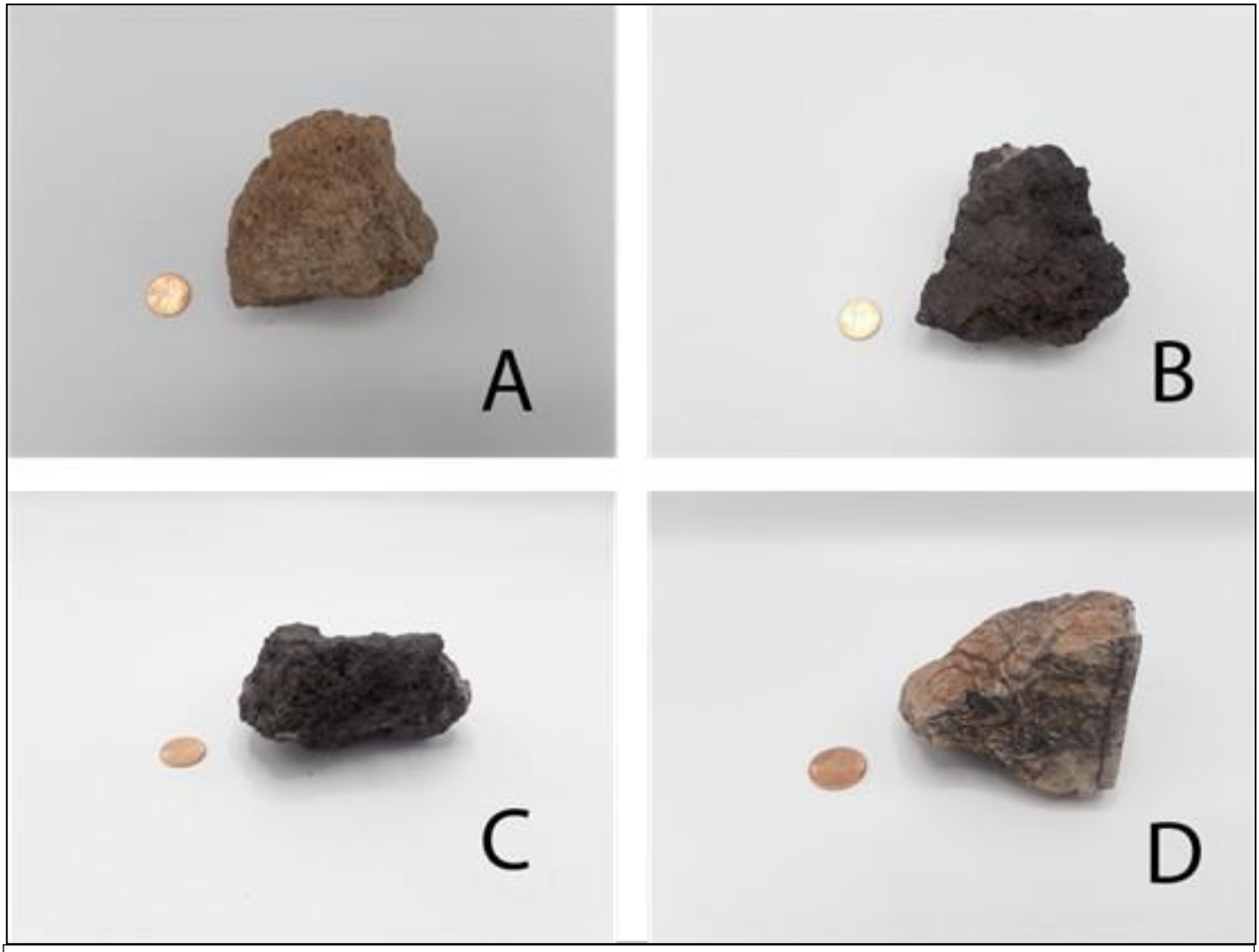

Figure 6. Hand sample images of the Purico pumice. (a) dacite, (b,c), andesite, (d)mingled andesite and dacite pumice. All samples were collected at -23°S -67.75°W in Northern Chile.

Figure 7. Example of glomerocryst observed in all of the andesite samples with plagioclase, pyroxene, and Fe-Ti oxides.

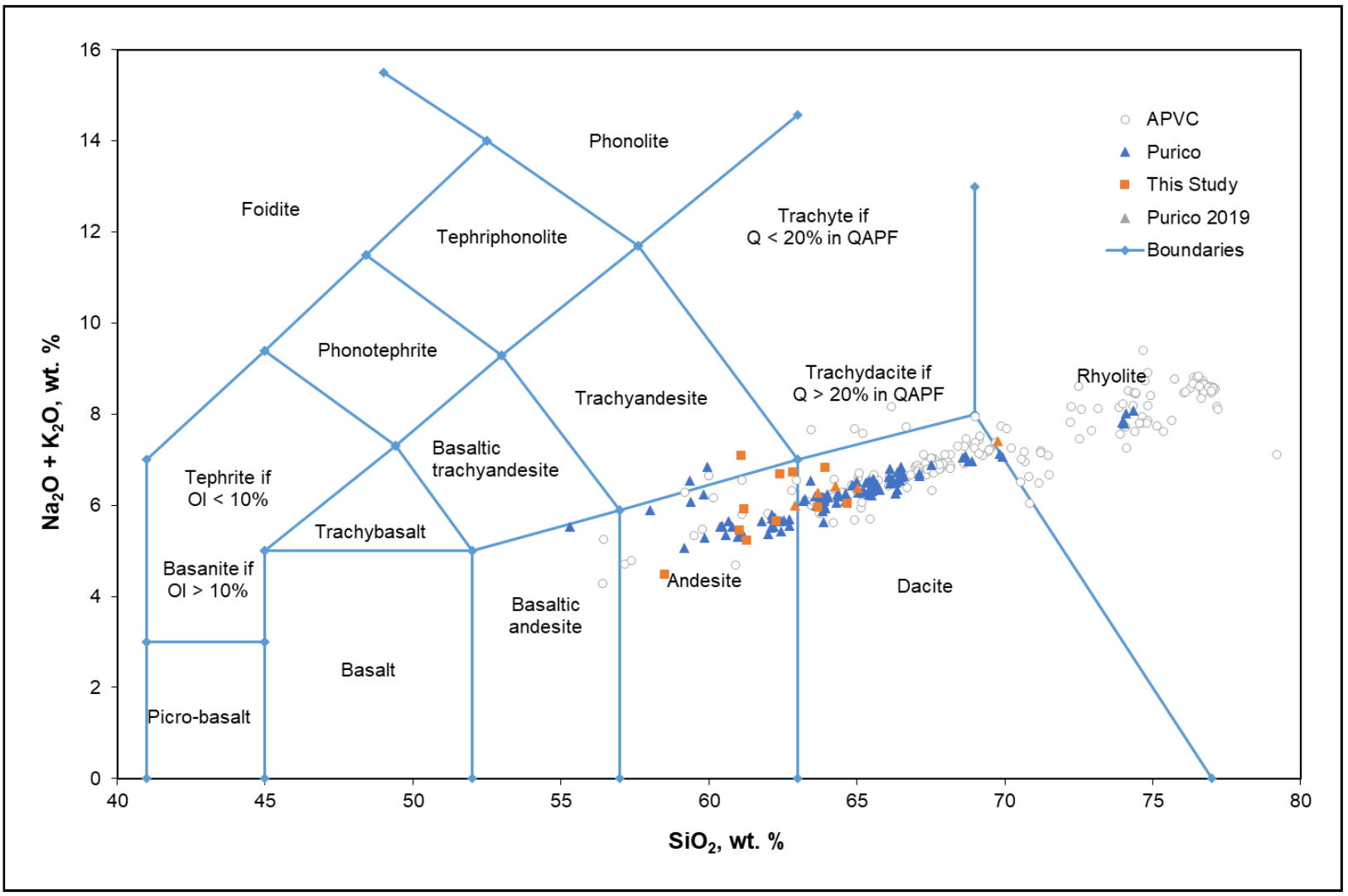

Figure 8. TAS diagram of whole rock compositions of the Altiplano Puna Volcanic Complex (APVC). The orange boxes indicate the samples analyzed in this study. The dacitic compositions in this study were found as bands in mingled pumice. The Purico andesite makes up some of the most mafic material found in the APVC.

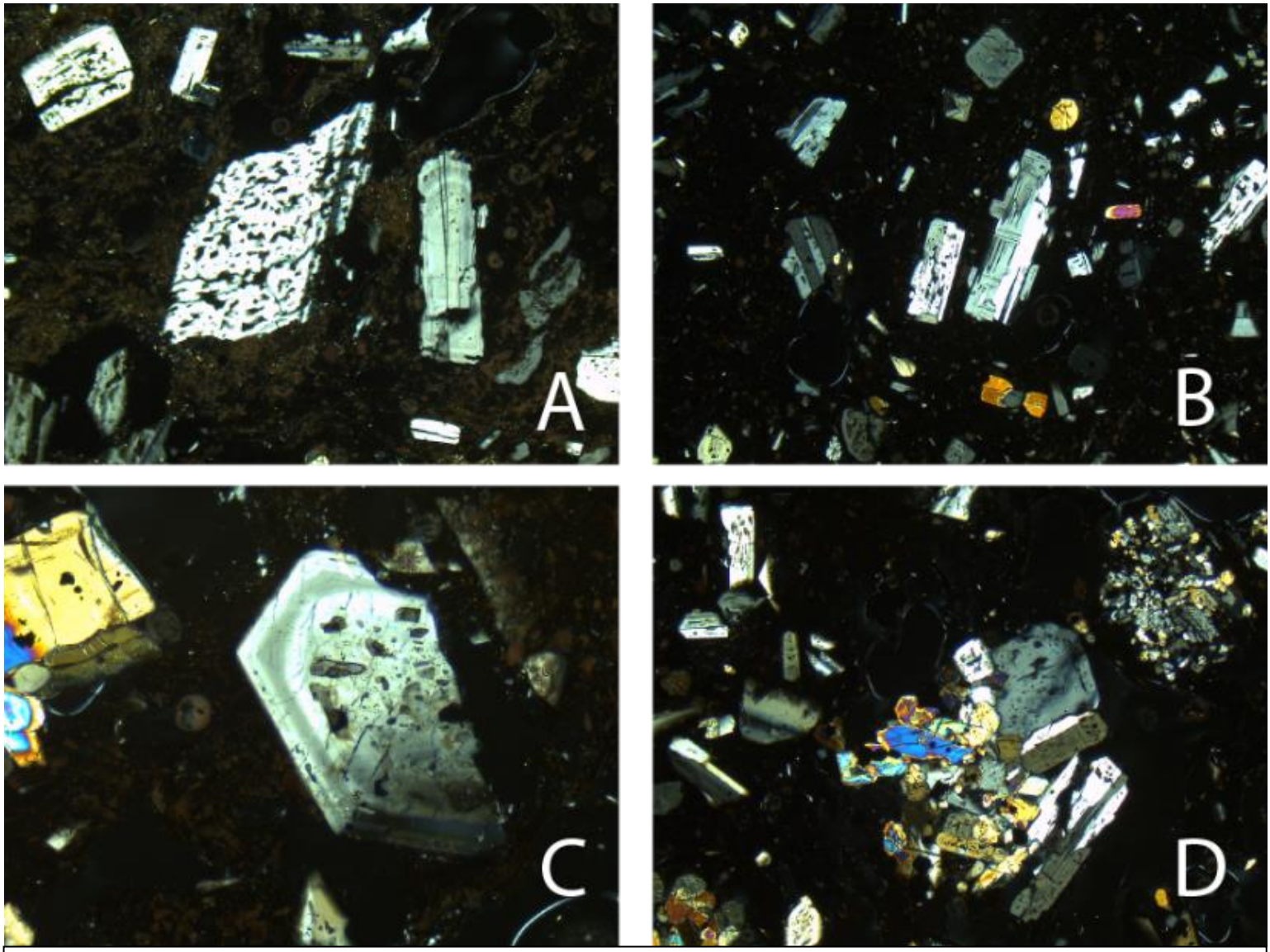

Figure 9. Different textures of plagioclase. (a) P2 plagioclase on the left showing extensive sieving. Plagioclase on the right with elongated crystals, albite twinning, and little sieving. (b) Elongate plagioclase with albite twinning and sieving. (c) Plagioclase with sieved core and displaying oscillatory zoning. (d) P1 plagioclase within a glomerocryst with OPX and CPX.

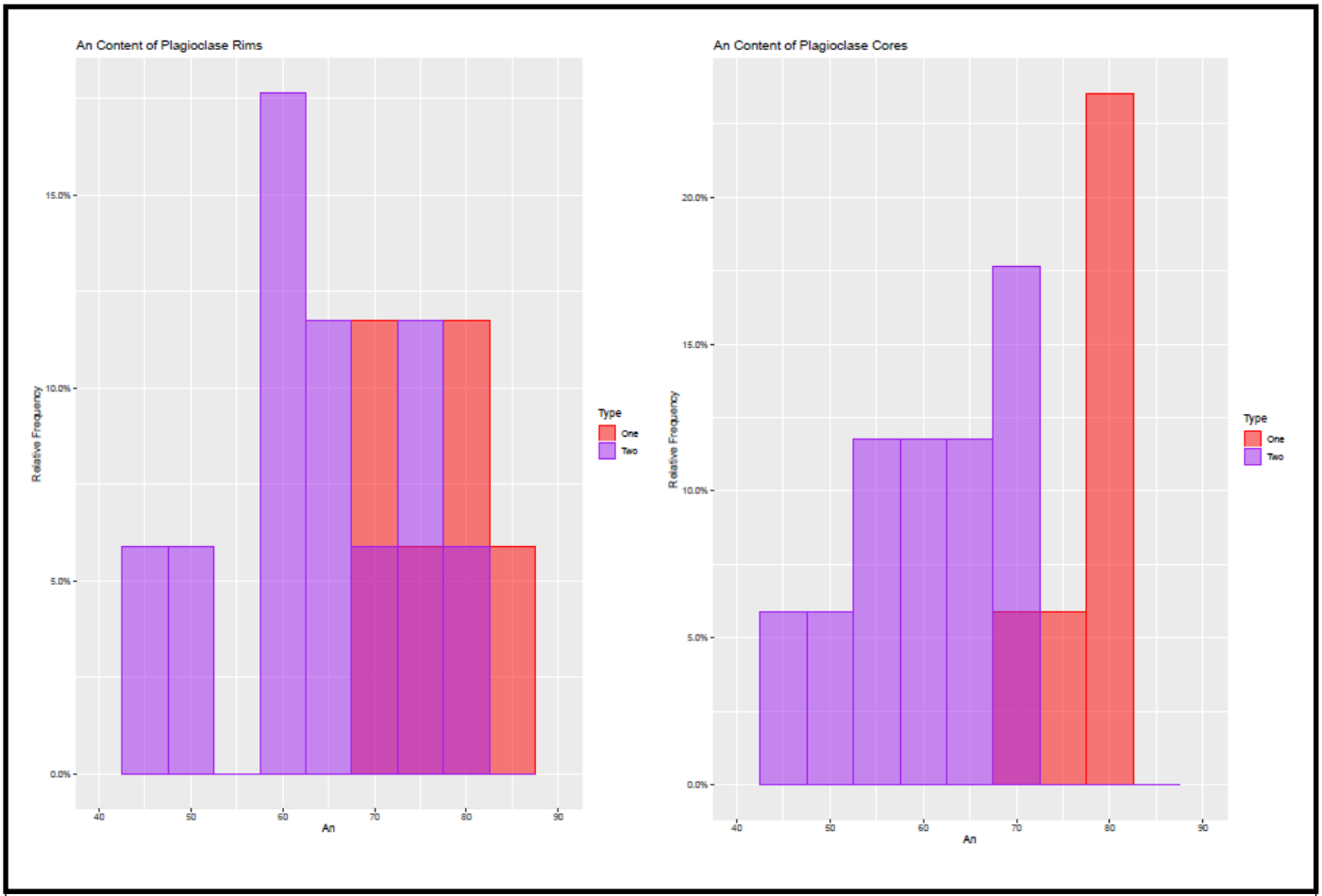

Figure 10. Histogram of plagioclase core and rim compositions of type P1 and P2 plagioclase. P1 has moderately higher An cores and significantly higher An rims.

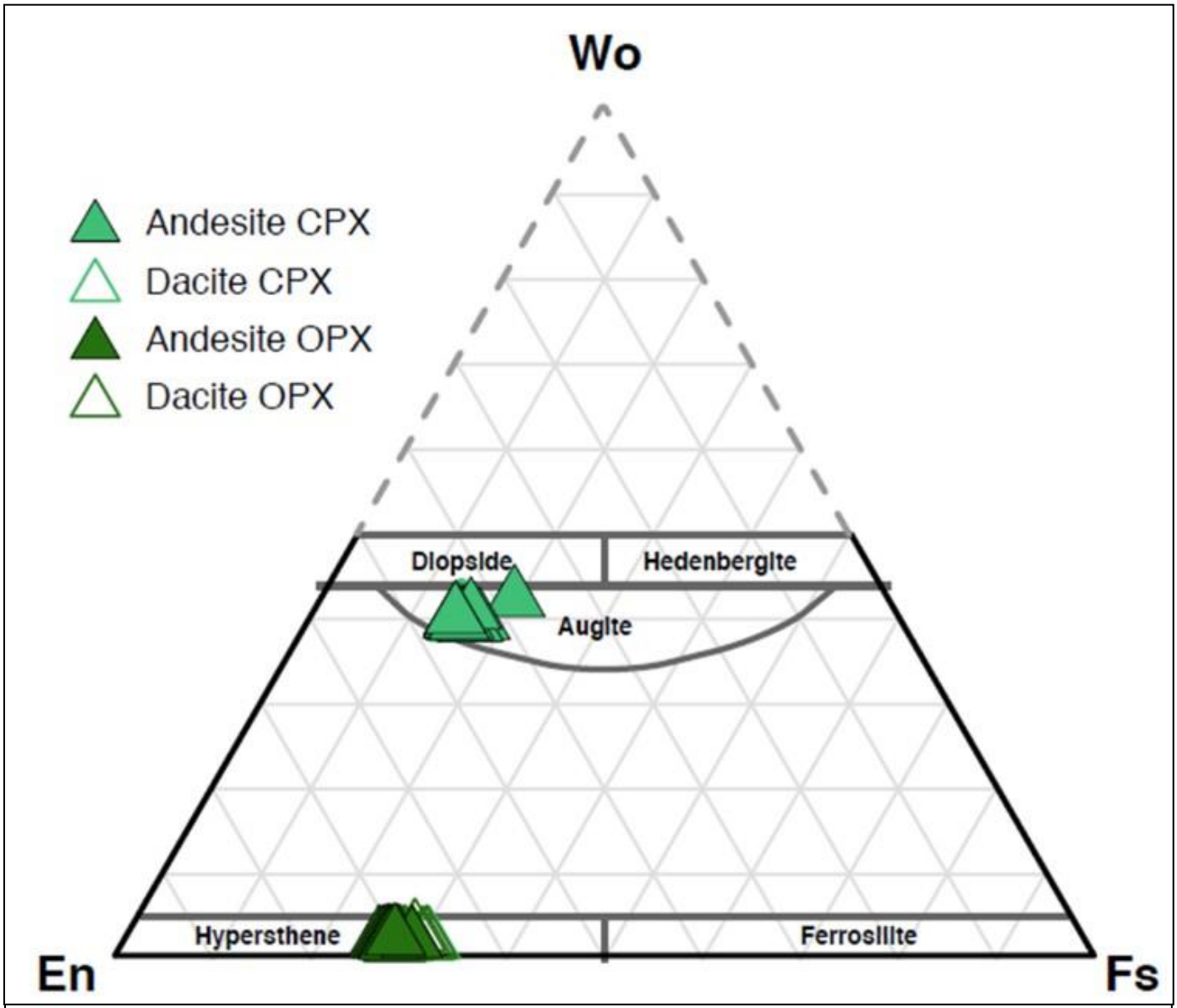

Figure 11. Ternary diagram of pyroxene compositions in the andesite and dacite.

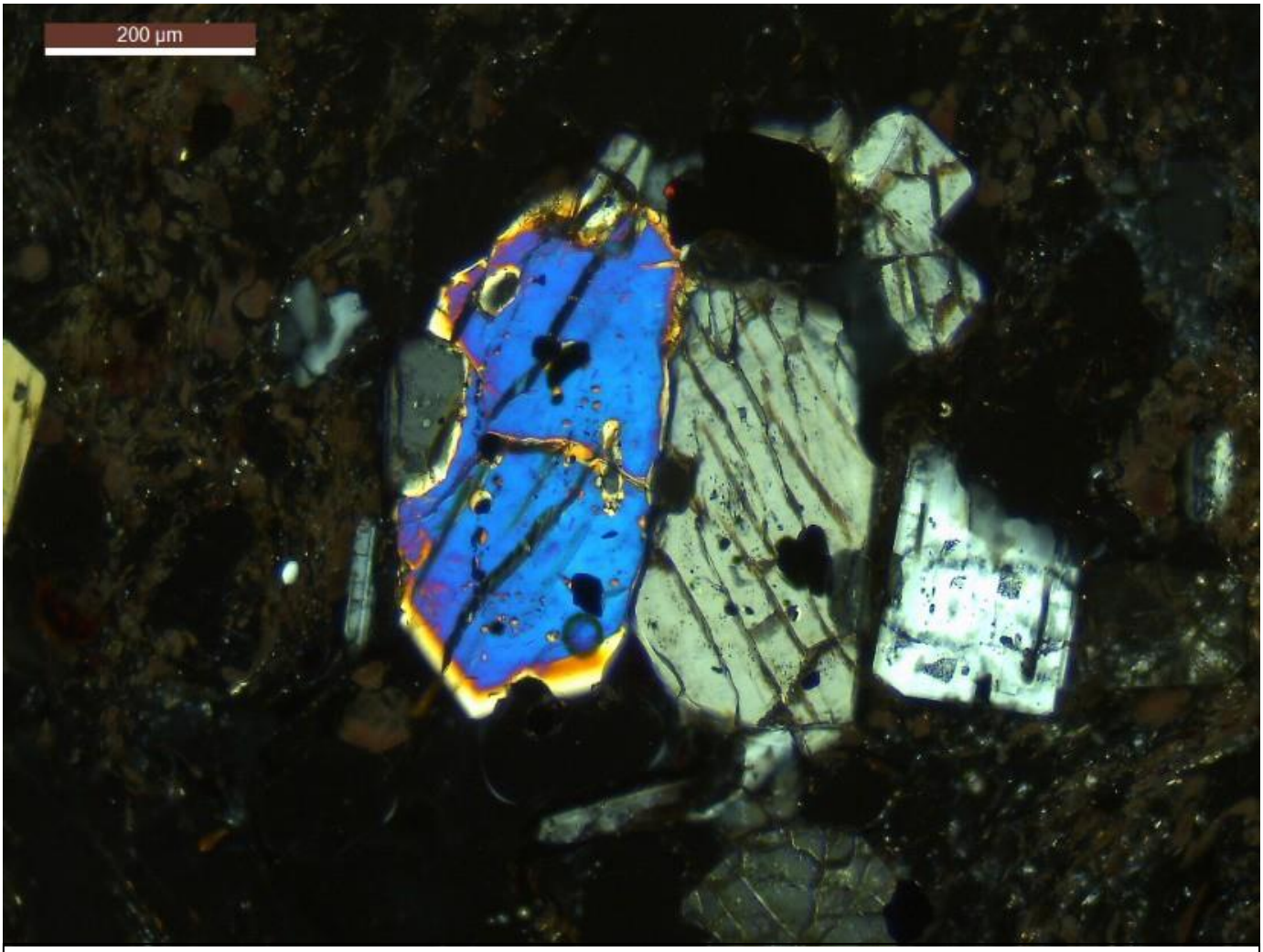

Figure 12. Touching pair of augite (CPX) (left) and hypersthene (OPX) (right) with melt and oxide inclusions in the andesite.

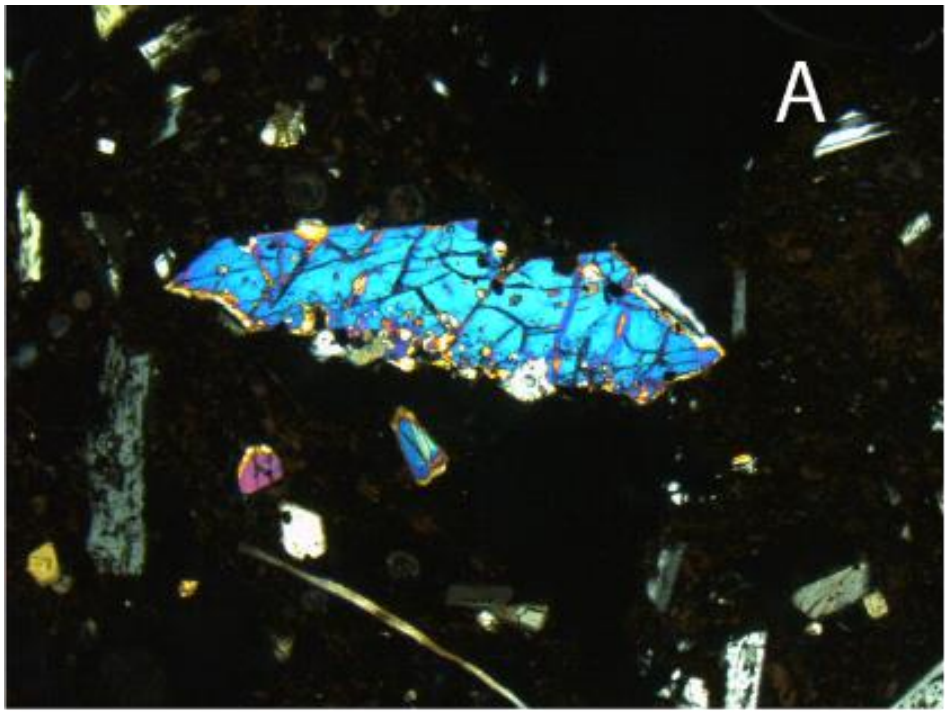

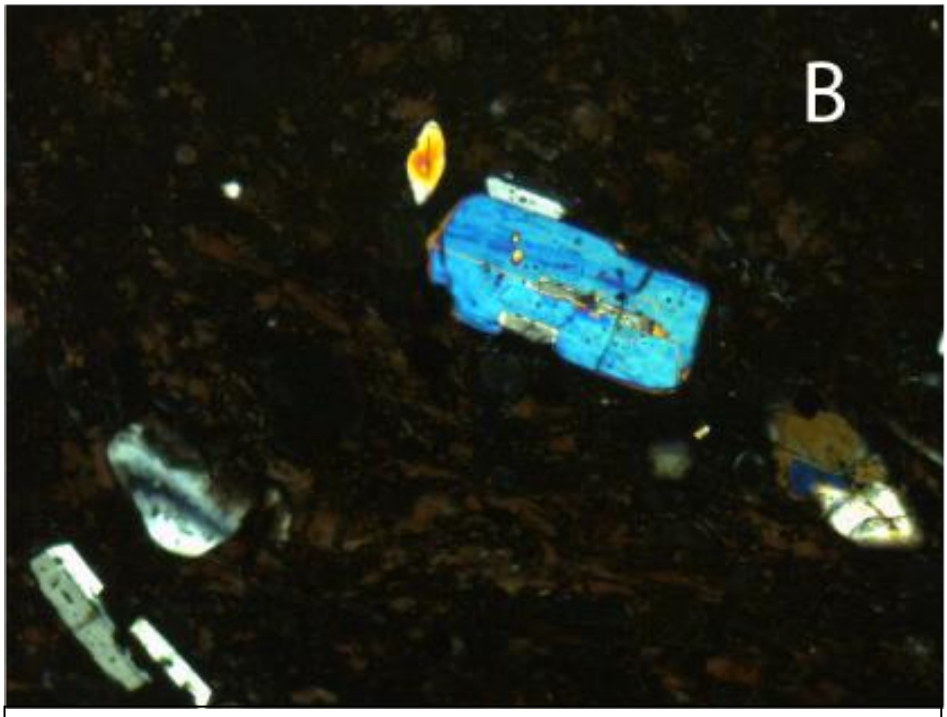

Figure 13. (a).Type 1 CPX. Large anhedral crystals with melt inclusions and sieved rims. (b) Type 2 CPX. Small phenocrysts with fewer melt inclusions and clear rims.

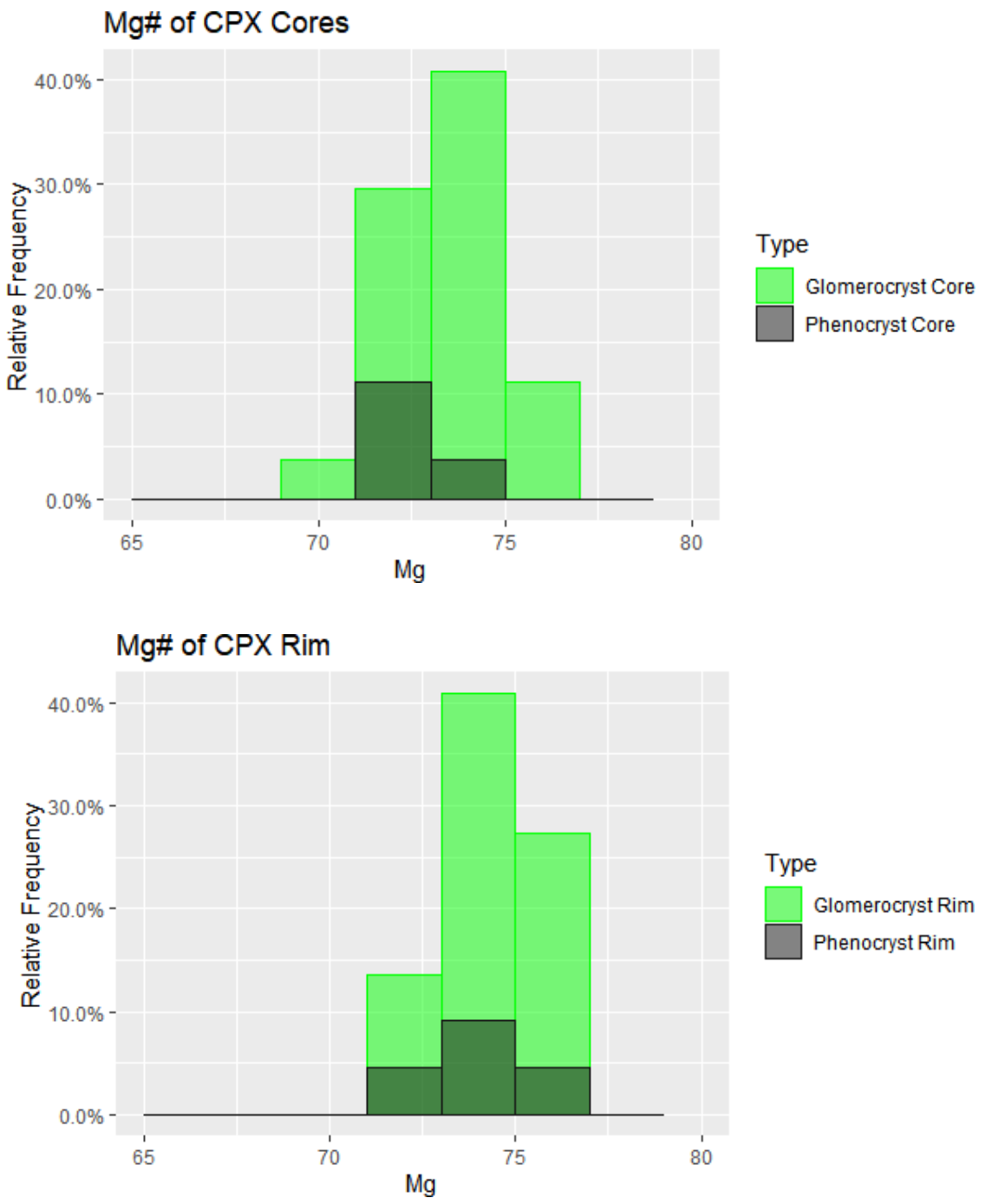

Figure 14. Histogram of clinopyroxene (CPX) core and rim compositions of CPX in glomerocrysts and phenocrysts. No observable compositional difference between glomerocrysts and phenocrysts. Glomerocryst cores had a slightly larger range of Mg#, CPX rims contained similar compositions as both glomerocrysts and phenocrysts.

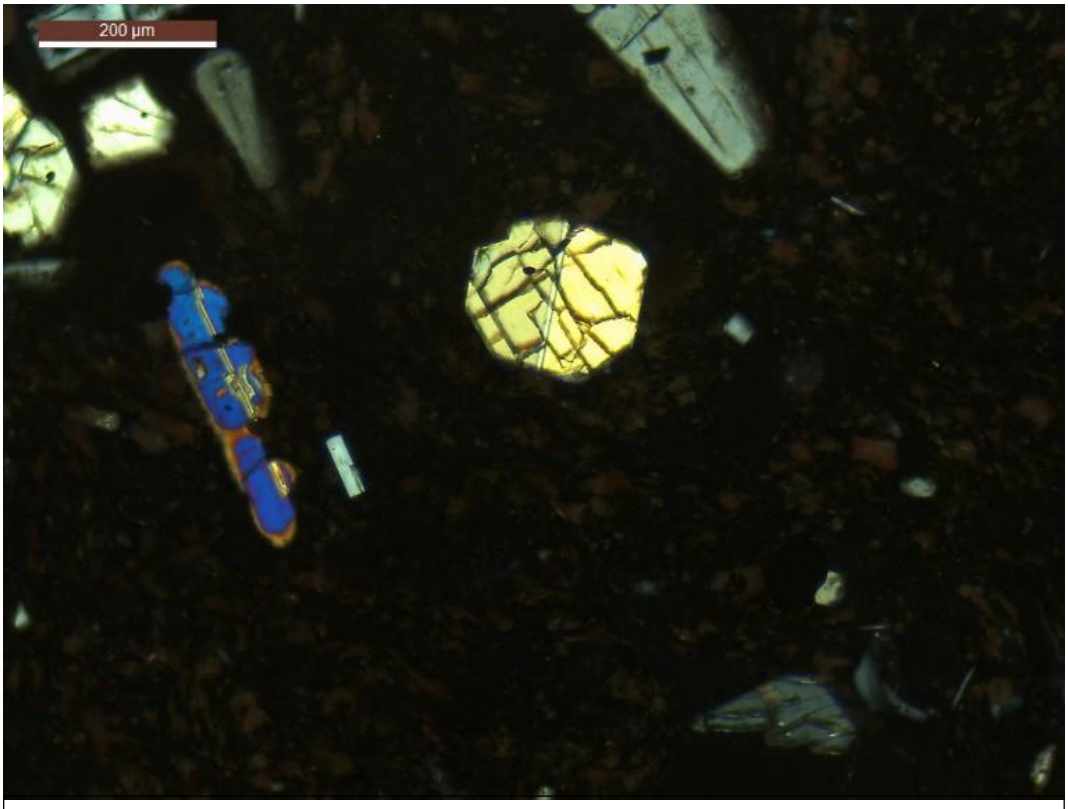

Figure 15. Orthopyroxene phenocryst in andesite thin section.

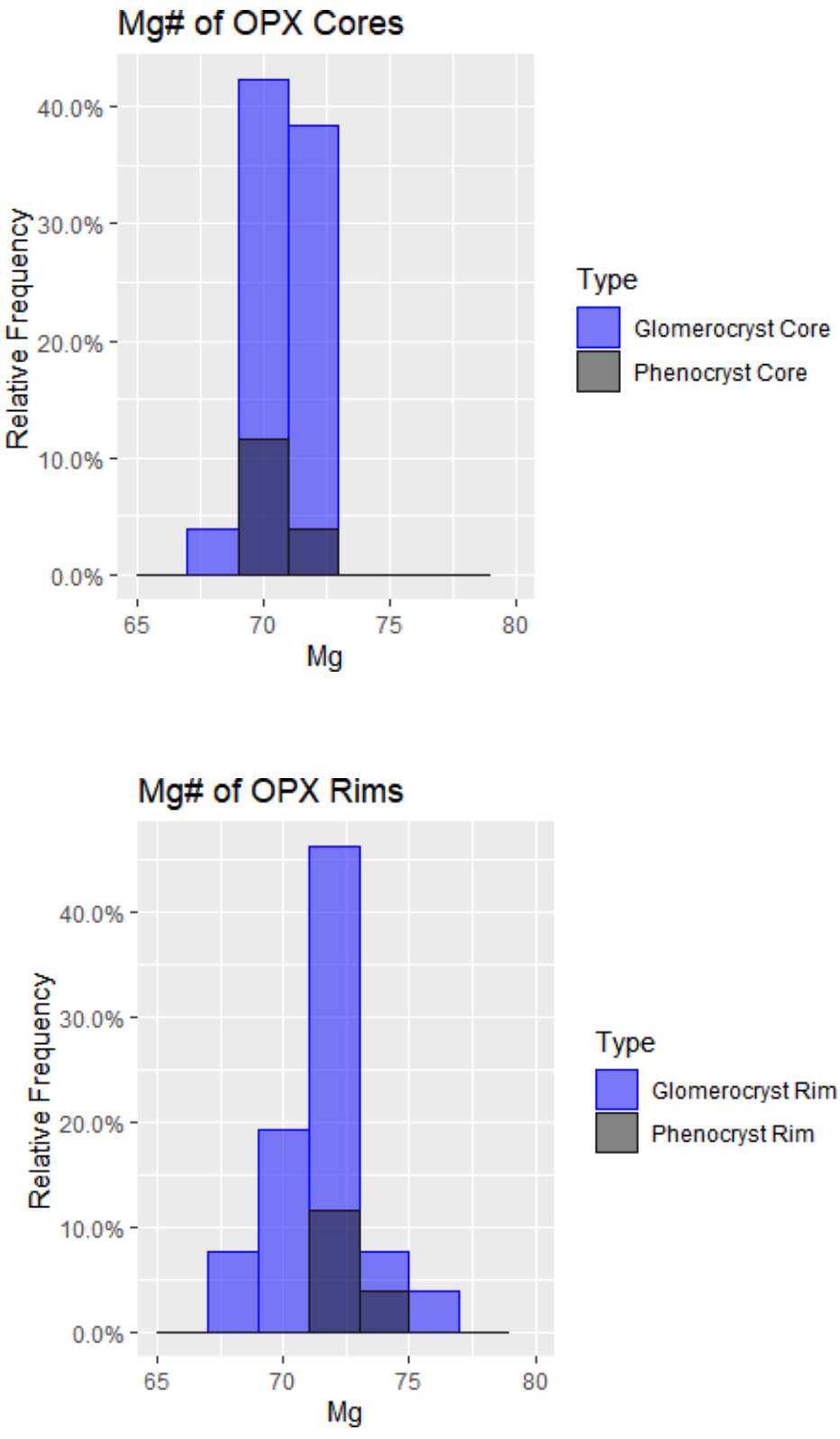

Figure 16. Histogram of Mg# of the orthopyroxene (OPX) glomerocrysts and phenocrysts. Glomerocrysts display a larger range of Mg# in the rims.

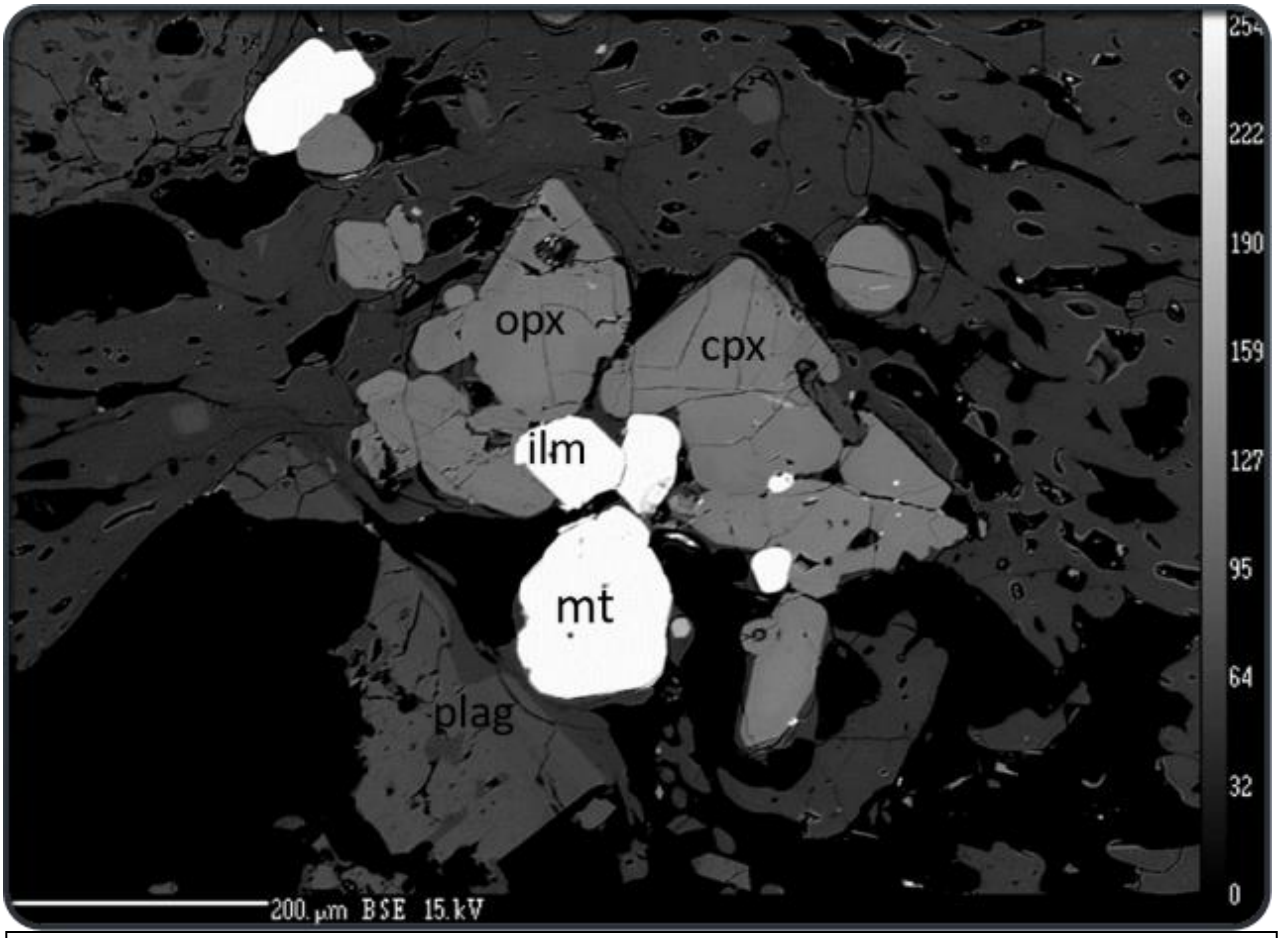

Figure 17. Backscatter electron (BSE) image of touching magnetite and ilmenite pairs in a glomerocryst.

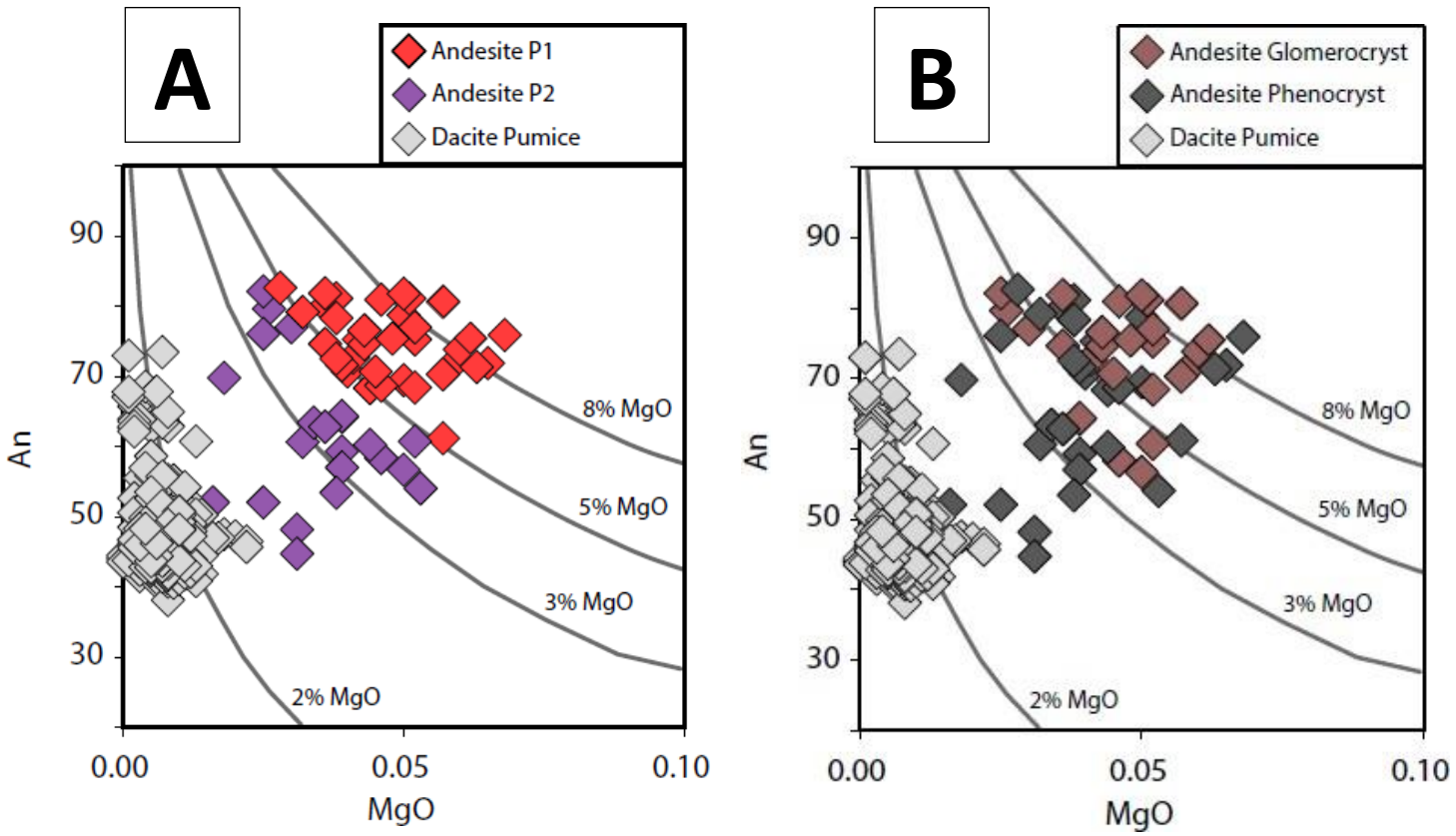

Figure 18. An vs MgO graph of Purico andesite and dacite pumice. (a) Plagioclase type 1 has significantly higher MgO and An values. (b) Phenocrysts and glomerocrysts cover a range of compositions. The andesite has higher MgO values and covers a larger range compared to the dacite.

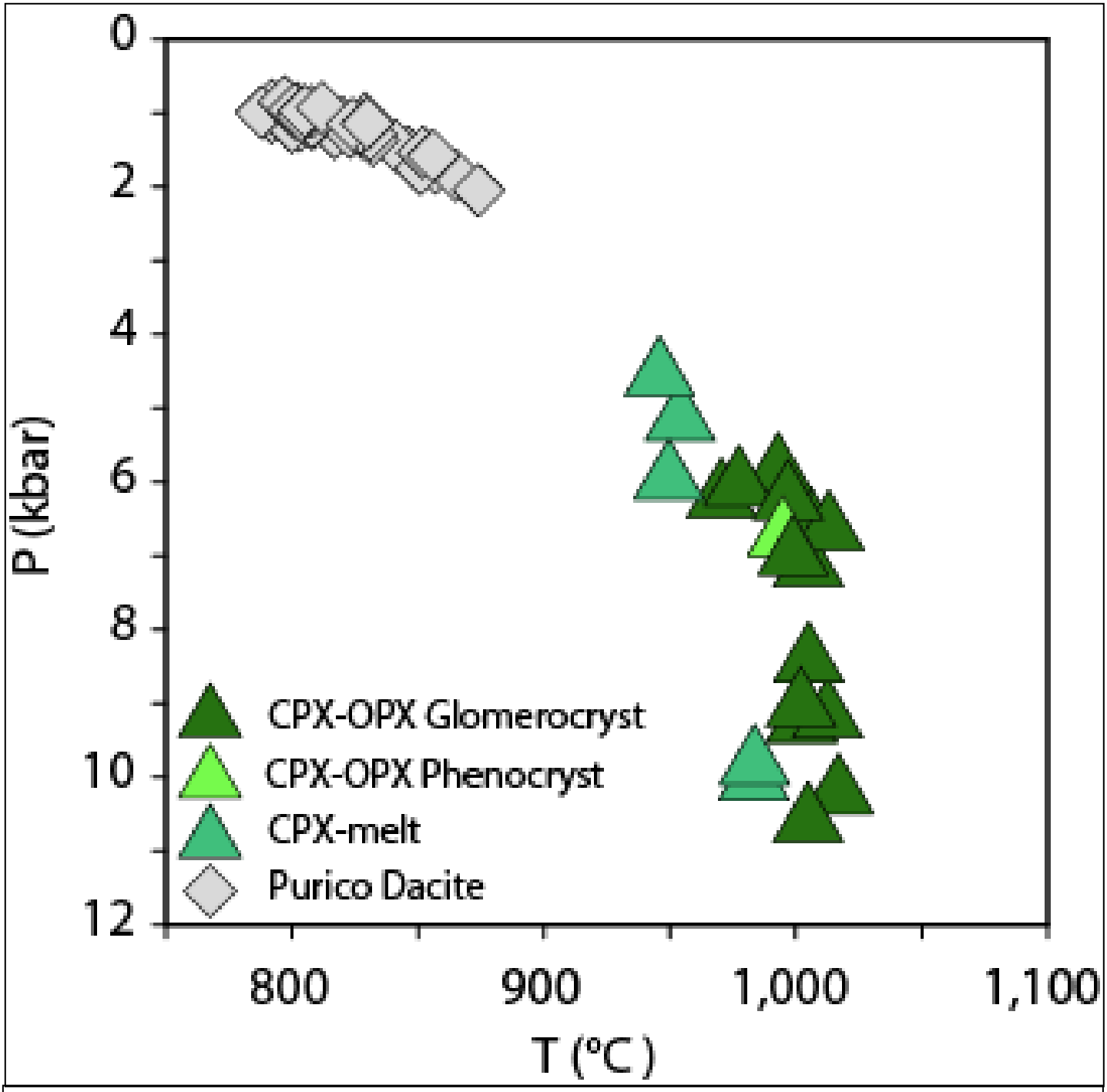

Figure 19. Two pyroxene and Cpx-melt geothermobarometry combined with amphibole and amphibole-plagioclase geothermobarometry from the dacites yield model estimates of pressure and temperature of crystallization.

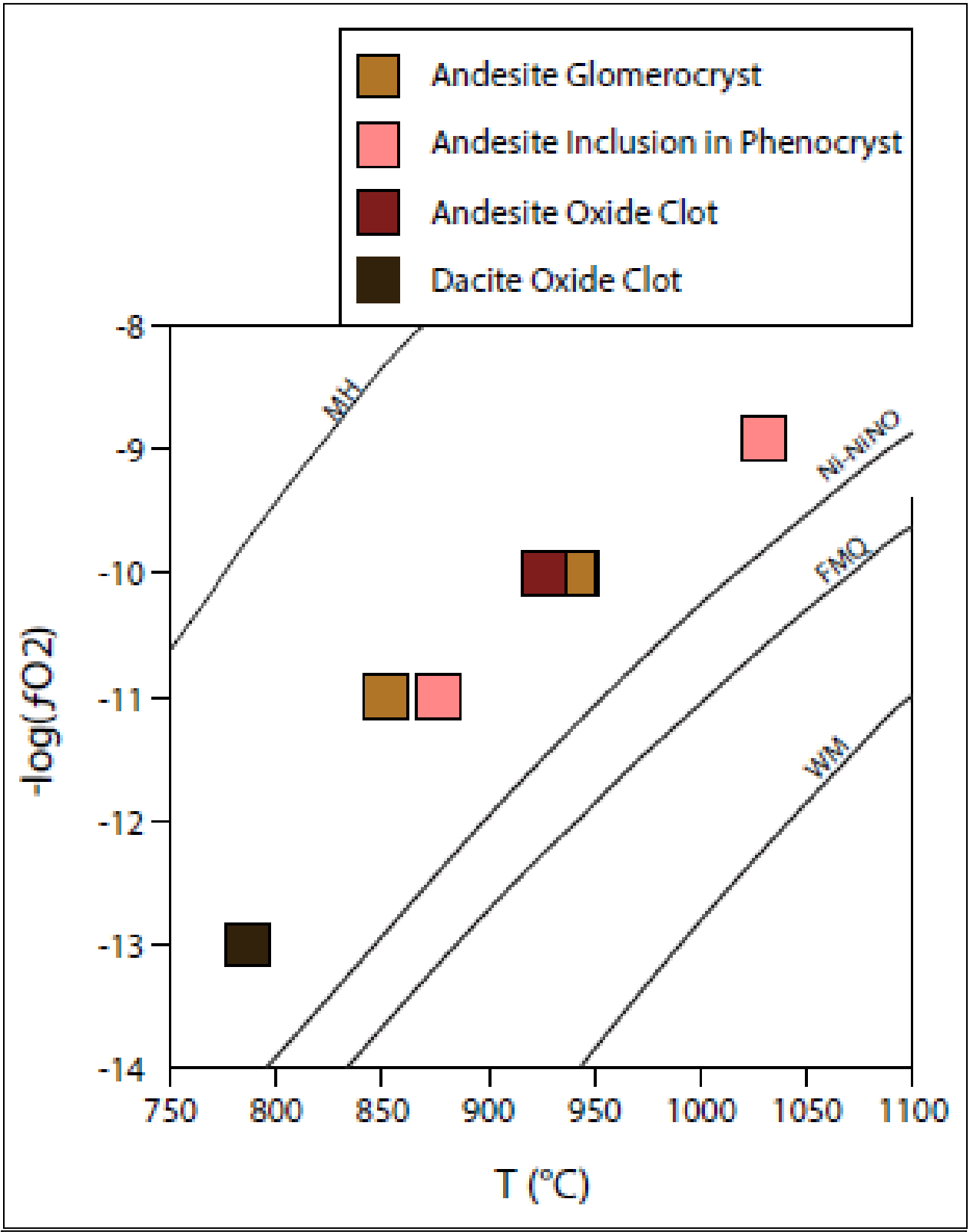

Figure 20. Temperature and oxygen fugacity of touching iron-titanium (Fe-Ti) oxide pairs determined with the ILMAT iron-titanium oxide thermometer (Lepage 2003).

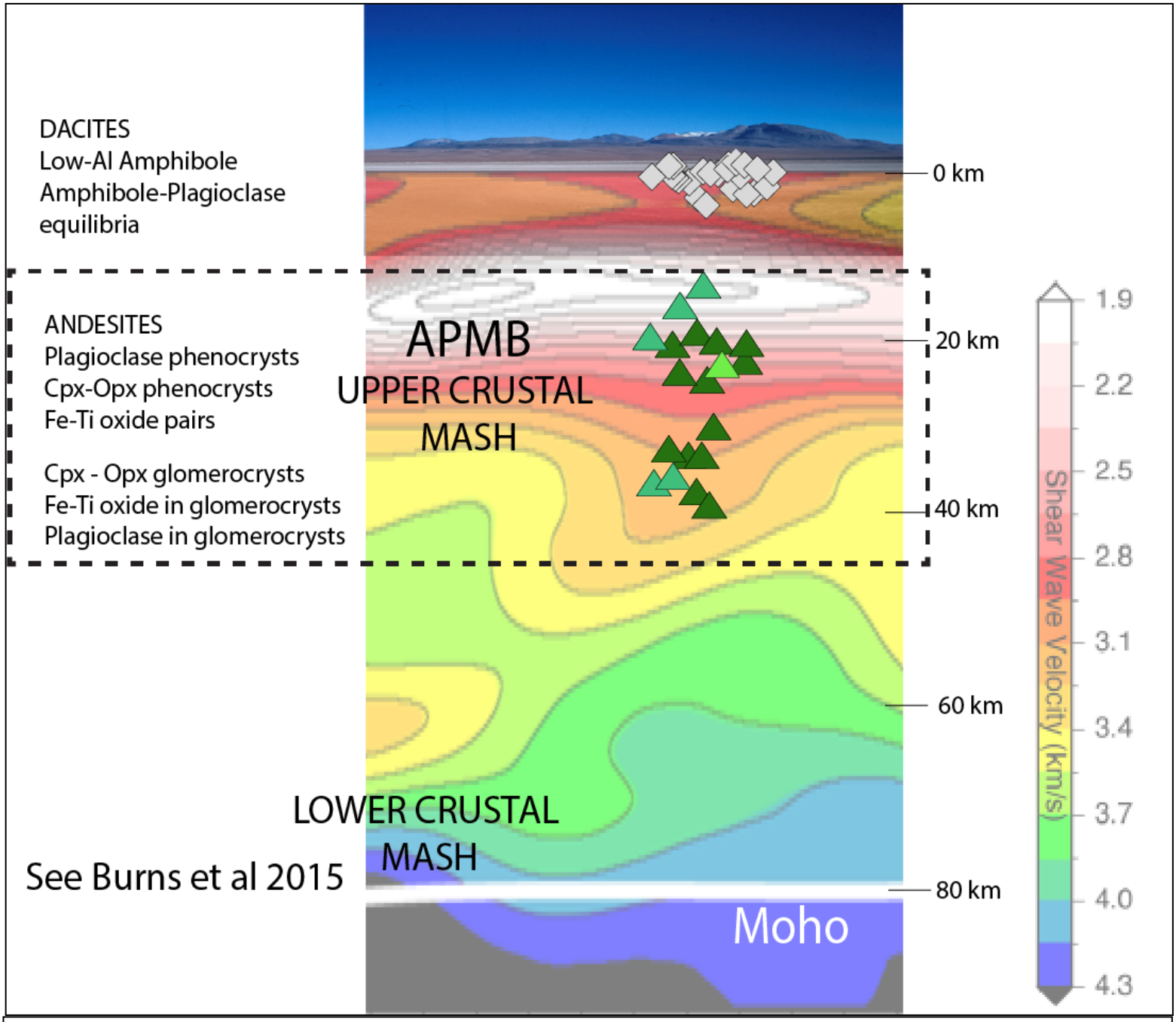

Figure 21. Thermobarometric depth estimations of the dacitic plagioclase-amphibole pairs and the andesitic pyroxene pairs overlain on a seismic cross section of Purico Volcanic Complex. The pyroxene pair's plot within the 2.9 km/s seismic boundary that represents the location of the APMB (Burns et. al. 2015).

Table 1. Petrographic Description of Purico Pumice

Rock Type	Proportions	Mineral Modal Percentages
Andesite	45-55% Crystals 30-40% Glass 10-15% Vesicles	15% Opx 10% Cpx 70% Plag 5% Fe-Ti Oxides
Dacite	40% crystals 40% Glass 15% Vesicles	10% Opx 10% Cpx 75% Plag 5% Fe-Ti Oxides
Banded Andesite Type I	60% Crystals 30% Glass 10% Vesicles	12% Opx 12% Cpx 50% Plag 16% Hornblende 5% Fe-Ti Oxides
Banded Andesite Type II	30% Crystals 50% Glass 30% Vesicles	80% Plagioclase 20% Biotite

Table 2. Whole-rock analysis of andesite and banded andesite Purico pumice

	CH12PIG001	CH12PIG003	CH12PIG004	CH12PIG005 Light Band	CH12PIG005 Dark Band	P8807	P8811 Light Band	P8811 Dark Band
SiO2	63.92458218	62.39679178	61.1006	62.28010653	61.18167061	61.29828032	64.6878	63.67802
TiO2	0.73	0.78	0.81	0.80	0.83	0.85	0.71	0.74
Al2O3	15.65	15.92	16.07	16.12	16.27	16.45	15.97	16.19
FeO*	4.72	5.22	5.71	5.66	5.85	6.17	4.87	5.14
MnO	0.08	0.09	0.10	0.10	0.10	0.11	0.09	0.09
MgO	2.54	2.89	3.23	3.23	3.42	3.54	2.39	2.66
CaO	5.35	5.84	5.70	5.96	6.24	6.16	4.92	5.28
Na2O	3.77	3.82	4.57	3.08	3.46	2.88	2.93	2.95
K2O	3.05	2.86	2.51	2.57	2.46	2.35	3.10	3.00
P2O5	0.17	0.18	0.19	0.20	0.19	0.20	0.33	0.27
Total	100.00	100.00	100.00	100.00	100.00	100.00	100.00	100.00
Ni	7.13	6.24	7.26	8.30	8.25	10.20	7.71	7.68
Cr	33.87	38.86	47.16	42.45	40.95	51.69	33.00	37.46
Sc	13.87	14.21	15.72	16.75	17.25	18.71	12.73	14.36
V	141.95	138.95	187.21	197.45	187.95	160.74	113.35	122.55
Ba	448.74	413.13	391.28	399.45	397.50	409.74	565.00	510.32
Rb	116.28	106.07	99.40	101.77	96.73	94.19	134.60	125.27
Sr	319.64	332.79	337.85	323.45	340.15	368.35	349.30	351.12
Zr	151.03	142.78	132.13	132.43	133.31	135.01	147.66	146.60
Y	23.27	22.62	21.64	21.85	21.65	21.99	20.25	21.80
Nb	11.21	10.05	9.80	9.50	9.75	9.50	11.79	10.92
Ga	18.14	16.88	17.86	17.50	17.20	18.51	17.88	17.85
Cu	8.59	12.18	20.85	14.35	23.55	36.77	16.93	9.73
Zn	58.19	62.42	71.59	65.15	69.30	79.40	68.51	73.61
Pb	16.99	16.34	12.39	16.95	14.30	11.04	16.32	17.51
La	28.50	25.64	25.62	26.30	25.15	24.68	30.03	28.50
Ce	57.28	53.96	49.95	51.40	50.15	52.19	61.46	60.44
Th	13.62	13.02	11.99	12.95	11.25	11.44	19.14	16.31
Nd	26.28	23.07	22.64	22.40	23.90	24.18	24.84	25.63
U	5.83	5.49	5.02	5.55	4.45	4.78	6.70	6.58

Table 3. Summary of the compositional plagioclase types

Unit	Purico	
Crystal Type	P1	P2
Size (um)	300-500	200-1000
Shape	subhedral	subhedral
Texture	clear and sieved	clear and sieved
An Core (wt%)	69-82	62-82
An Rim (wt%)	55-68	43-54
MgO (wt%)	0.59-0.68	0.35-0.51
FeO (wt%)	0.55-0.70	0.30-0.49

Table 4. Representative compositions of plagioclase from the Purico Ignimbrite

Sample	phenocryst CH12PIG002		glomerocryst P8810	
	Core	Rim	Core	Rim
SiO2	49.99	49.21	48.14	49.13
TiO2	0.03	0.03	0.02	0.02
Al2O3	31.20	31.77	32.92	32.13
FeO	0.54	0.56	0.52	0.57
MnO				
MgO	0.05	0.06	0.05	0.05
CaO	14.21	15.04	16.26	15.22
Na2O	3.07	2.62	2.03	2.65
K2O	0.15	0.12	0.09	0.12
An	71.28	75.47	81.17	75.45
Ab	27.82	23.82	18.32	23.81
Or	0.89	0.71	0.51	0.73

Table 5. Summary of Pyroxene Compositions

	CPX	OPX
Size (um)	200-300	50-200
Texture	sieved rims with melt and oxide inclusions	sieved rims with melt and oxide inclusions
Wo (wt%)	39.5-40.5	1.76-3.77
Mg#	73-75	68.3-72.1